

1 **Diagnostic calibration of a hydrological model in a mountain**
2 **area by hydrograph partitioning**

3 Z. H. He¹, F. Q. Tian^{1*}, H. V. Gupta², H. C. Hu¹, H. P.Hu¹

4

5

6 1. State Key Laboratory of Hydrosience and Engineering, Department of Hydraulic
7 Engineering, Tsinghua University, Beijing 100084, China

8 2. Department of Hydrology and Water Resources, The University of Arizona,
9 Tucson, Arizona, 85721, USA

10

11 *Corresponding author information:

12 Email: tianfq@tsinghua.edu.cn

13 Tele: +86 010 6277 3396

14 Fax: +86 010 6279 6971

15

16

17

18 Manuscript submitted to Hydrology and Earth System Sciences

19 2015.03.02

20 **Abstract**

21 Hydrological modeling can exploit informative signatures extracted from long time sequences
22 of observed streamflow for parameter calibration and model diagnosis. In this study we explore
23 the diagnostic potential of hydrograph partitioning for model calibration in mountain areas,
24 where meltwater from snow and glaciers are important sources for river runoff (in addition to
25 rainwater). We propose an index-based method to partition the hydrograph according to
26 dominant runoff water sources, and a diagnostic approach to calibrate a mountain hydrological
27 model. First, by accounting for the seasonal variability of precipitation and the altitudinal
28 variability of temperature and snow/glacier coverage, we develop a set of indices to indicate
29 the daily status of runoff generation from each type of water source (i.e., glacier meltwater,
30 snow meltwater, rainwater, and groundwater). Second, these indices are used to partition a
31 hydrograph into four parts associated with four different combinations of dominant water
32 sources (i.e., groundwater, groundwater + snow meltwater, groundwater + snow meltwater+
33 glacier meltwater, groundwater + snow meltwater + glacier meltwater + rainwater). Third, the
34 hydrological model parameters are grouped by the associated runoff sources, and each group is
35 calibrated to match the corresponding hydrograph partition in a stepwise and iterative manner.
36 Similar to use of the regime curve to diagnose seasonality of streamflow, the hydrograph
37 partitioning curve based on a dominant runoff water source (more briefly called the partitioning
38 curve, not necessarily continuous) can serve as a diagnostic signature that helps relate model
39 performance to model components. The proposed methods are demonstrated via application of
40 a semi-distributed hydrological model (THREW) to the Tailan River basin (1324 km²) in the
41 Tianshan Mountain of China. Results show that the proposed calibration approach performed
42 reasonably well. Cross validation and comparison to an automatic calibration method indicated
43 its robustness.

44 **1 Introduction**

45 **1.1 Background**

46 Parameter calibration has been singled out as one of the major issues in the application of
47 hydrological models (Johnston and Pilgrim, 1976; Gupta and Sorooshian, 1983; Beven and
48 Binley, 1992; Boyle *et al.*, 2000). Commonly, one or more objective functions are selected as
49 criteria to evaluate the similarity between observed and simulated hydrographs (Nash and
50 Sutcliffe, 1970; Brazil, 1989; Gupta *et al.*, 1998; van Griensven and Bauwens, 2003). As model
51 complexity increases, parameter dimensionality also increases significantly, which makes it
52 much more difficult to calibrate model parameters manually. For this reason, automatic
53 calibration procedures have been developed to identify the optimal parameter set (Gupta and
54 Sorooshian, 1985; Gan and Biftu, 1996; Vrugt *et al.*, 2003a,b). However, due to limitations in
55 process understanding and measurement technologies, one can find different parameter sets
56 within a chosen space that may acceptably reproduce the observed aspects of the catchment
57 system (Sorooshian and Gupta, 1983; Beven and Freer, 2001). This phenomenon, which has
58 been called “equifinality”, causes uncertainty in simulation and prediction (Duan *et al.*, 1992;
59 Beven, 1993, 1996), and highlights the need for methods that are powerful enough to
60 ‘diagnostically’ evaluate and correct models, i.e., that are capable of indicating to what degree
61 a realistic representation of the real world has been achieved and pointing towards how the
62 model should be improved (Spear and Hornberger, 1980; Gupta *et al.*, 1998, 2008).

63 Traditional regression-based model evaluation strategies (e.g., based on the use of Mean
64 Squared Error or Nash Sutcliffe Efficiency as performance criteria) are demonstrably poor in
65 their ability to identify the roles of various model components or parameters in the model output
66 (Van Straten and Keesman, 1991; Zhang *et al.*, 2008; Gupta *et al.*, 2008; Yilmaz *et al.*, 2008;
67 Hingray *et al.*, 2010), which is due in part to the loss of meaningful information when projecting
68 from the high dimension of the data set (like hydrograph) down to the low (often one)
69 dimension of the measure (Yilmaz *et al.*, 2008; Gupta *et al.*, 2009). A diagnostic evaluation
70 method should match the number of unknowns (parameters) with the number of pieces of
71 information by making use of multiple measures of model performance (Gupta *et al.*, 1998,
72 2008, 2009; Yilmaz *et al.*, 2008). One way to exploit hydrological information is to analyze the
73 spatiotemporal characteristics of hydrological variables that can be related to specific

74 hydrological processes in the form of “signature indices” (Richter *et al.*, 1996; Sivapalan *et al.*,
75 2003; Gupta *et al.* 2008, Yilmaz *et al.*, 2008). Ideally, a “signature” should represent some
76 “invariant” property of the system, be readily identifiable from available data, directly reflect
77 some system function, and be maximally related to some “structure” or “parameter” in the
78 model.

79 Attention to hydrological signatures, therefore, constitutes the natural basis for model
80 diagnosis (Gupta *et al.*, 2008). Placed in this context, the body of literature on the topic is indeed
81 large. Jothityangkoon *et al.* (2001) proposed a downward approach to evaluate the model’s
82 performance against appropriate signatures at progressively refined time scale. Signatures that
83 govern the evaluation of model complexity are the inter-annual variability, mean monthly
84 variation in runoff (called regime curve), and the flow duration curve (FDC). Farmer *et al.*
85 (2003) evaluated the climate, soil and vegetation controls on the variability of water balance
86 through four signatures: gradient of the annual yield frequency graph, average yield over many
87 years for each month, FDC, and magnitude and shape of the hydrograph. Shamir *et al.* (2005a)
88 described a parameter estimation method based on hydrograph descriptors (total flow, range
89 between the extreme values, monthly rising limb density of the hydrograph, monthly maximum
90 flow and negative/positive change) that characterize dominant streamflow patterns at three
91 timescales (monthly, yearly, and record extent). Detenbeck *et al.* (2005) calculated several
92 hydrologic indices including daily flow indices (mean, median, coefficient of variation, and
93 skewness), overall flood indices (flood frequency, magnitude, duration, and flood timing of
94 various levels), low flow variables (mean annual daily minimum), and ranges of flow
95 percentiles to study the relationship of the streamflow regime to watershed characteristics.
96 Shamir *et al.* (2005b) presented two streamflow indices to describe the shape of the hydrograph
97 (rising/declining limb density, i.e., RLD and DLD) for parameter estimation in 19 basins of
98 United States. Yadav *et al.* (2007) used similarity indices and hydrological signatures (runoff
99 ratio and slope of the FDC) to classify catchments. Westerberg *et al.* (2011) selected several
100 evaluation points on the FDC to calibrate models, and compared two selection methods to
101 evaluate their effects on parameter calibration.

102 Generally, the reported signatures have the following two characteristics: (1) they
103 concentrate on the extraction of hydrologically meaningful information contained in

104 hydrographs, and (2) they focus on either an entire study period or a special continuous section
105 of the entire period. They have occasionally considered temporal variability of runoff
106 components and dominance of different runoff sources during different periods (e.g., the
107 seasonal switching of runoff sources discussed in Tian *et al.*, 2012). However, a hydrograph
108 could be dominated by various components or water sources at different response times
109 (Haberlandt *et al.*, 2001; Eder *et al.*, 2005). Within this in mind, a few studies have explored
110 the use of hydrological information in time dimension for stepwise calibration. For example,
111 Schaefli *et al.* (2005) presented a stepwise calibration method for 7 parameters in a high
112 mountainous area: snow and ice melt degree-day factors were conditioned by mass balance,
113 slow reservoir parameters were determined by base flow, reservoir coefficients were calibrated
114 by summer runoff, and the direct runoff coefficient was used to control discharge during
115 precipitation events. Another notable example is Hingray *et al.* (2010), in which the authors
116 estimated the value of snowmelt degree-day factor in a mountain basin by progressively
117 minimizing the differences between observed and simulated values of different magnitude
118 hydrographs. There are also many other follow up studies.

119 In mountain areas, streamflow is composed of both snow/glacier meltwater and rainwater.
120 The energy-based and temperature-index models are two principal approaches to simulate snow
121 and glacier melt (Rango and Martinec, 1979; Howard, 1996; Kane *et al.*, 1997; Singh *et al.*,
122 2000; Fierz *et al.*, 2003). To describe significant heterogeneity of temperature, precipitation,
123 snow, and glacier, distributed hydrological models are generally used for precipitation-runoff
124 modeling in mountain regions (Daly *et al.*, 2000; Klok *et al.*, 2001 etc.). Also, the utilization of
125 remotely sensing products of precipitation and snow cover data in the mountain runoff
126 modeling has become more popular in recent years (Swamy and Brivio, 1997; Akyurek *et al.*,
127 2011; Liu *et al.*, 2012 etc.). Most of these studies report sound simulation results. However, the
128 need to develop an appropriate calibration strategy for precipitation-runoff modeling in
129 mountain areas remains a key issue for two reasons: first, the hydrological processes are usually
130 more complex (with snow/glacier melt and possibly soil freezing/thawing) than those in warmer
131 areas, which implies a larger dimension of parameter (R^P) in the corresponding hydrological
132 model; second, measured data set useful for model identification is usually limited due to a
133 sparse gauge network, which produces a small measurement dimension (R^M) far lower than R^P .

134 To address this problem, related studies are putting effort into two directions. One is to reduce
135 the calibrated R^P by estimating some of the parameters based on basin characteristics *a priori*.
136 For example, Gurtz *et al.* (1999) proposed a parameterization method based on elevation, slope
137 and shading derived from basin terrain. Gomez-Landes and Rango (2002) obtained model
138 parameters of ungauged basins from gauged basins by basin size, proximity of location, and
139 shape similarities. Eder *et al.* (2005) estimated most of the parameters *a priori* from basin
140 physiography before an automatic calibration was applied. The parameterization method may
141 involve some uncertainties but be useful for the determination of insensitive parameters.

142 The second direction is to exploit hydrological information from implicit measure data.
143 For instance, Dunn and Colohan (1999) used baseflow data as additional criteria for model
144 evaluation. Mendoza *et al.* (2003) exploited recession-flow data to estimate hydraulic
145 parameters. Stahl *et al.* (2008) used glacier mass balance information combined with stream
146 hydrographs to constrain melt factors. Huss *et al.* (2008) used annual ice volume change data
147 for optimizing melt and radiation factors, and glacier equilibrium line altitude for precipitation
148 correction factors. Schaepli and Huss (2011) integrated the seasonal information of point glacier
149 mass balance for model calibration by modifying the GSM-SOCONT model. Jost *et al.* (2012)
150 introduced glacier volume loss calculated by high-resolution digital elevation models to
151 calibrate hydrologic model. Knowledge acquired from the aforementioned research indicates
152 that the use of additional information (e.g., baseflow, recession flow, and glacier mass balance)
153 can effectively help reduce parameter uncertainty by significantly expanding R^M .

154 However, glacier mass data and baseflow data are usually not available in some mountain
155 basins. In these cases, hydrograph partitioning is another possible way to exploit information
156 from available data. Information about dominant hydrological processes contained in a
157 hydrograph can be extracted by hydrograph partitioning or separation; this has long been a topic
158 of interest in hydrology. Several different kinds of methods have been proposed (Pinder and
159 Jones, 1969; McCuen, 1989; Nathan, 1990; Arnold *et al.*, 1995, 1999; Vivoni *et al.*, 2007),
160 which can generally be classified into graphical methods, analytical methods, empirical
161 methods, geochemical methods and automated program techniques (Nejadhashemi *et al.*, 2009).
162 Most of them primarily focus on the partitioning of baseflow and are not capable of identifying
163 more than two components. With the advent of isotope methods, multi-component hydrograph

164 separation models have been developed. However, these models need be run for an extended
165 period of time (usually a minimum of one hydrologic year) for the assumption that the isotopes
166 of components are conserved to hold (Hooper and Shoemaker, 1986) and call for volumes of
167 field data that are seldom available in poorly gauged and difficult to access mountain basins.

168 **1.2 Objectives and Scope**

169 This paper explores the benefits of partitioning the hydrograph into several parts, each
170 related to one combination of dominant water sources for runoff generation. The parameter
171 group controlling each type of runoff sources is then calibrated using the corresponding
172 partitioning hydrographic curves via a stepwise approach, and model deficiencies are diagnosed
173 by evaluating the model simulations associated with each partitioning curve (as a diagnostic
174 signature). We demonstrate the potential of this approach in a mountain area where streamflow
175 is the result of complex runoff generation processes arising from combinations of storm events
176 and snow/glacier melt. The influence of each type of water source (groundwater, snow
177 meltwater, glacier meltwater, or rainwater) varies in time and can be determined by an analysis
178 of the dynamic spatiotemporal information in the available data series.

179 The paper is organized as follows. Section 2 contains a description of the geographic and
180 hydrological characteristics of the study basin, including the main data sources and data
181 preprocessing. Section 3 details the proposed method of hydrograph partitioning and parameter
182 calibration based on a semi-distributed model coupled with the temperature-index method.
183 Section 4 presents the results and discusses the possible sources of uncertainty. Section 5
184 provides a summary of this study and discusses further applications of the partitioning strategy.

185 **2 Study Area and Data**

186 **2.1 Overview of the Study Area**

187 The study mountain area (Tailan River basin, TRB) is on the south slope of the Tianshan
188 Mountain (one of the highest mountain areas in China) in the Xinjiang Uygur Autonomous
189 Region of China and extends from 41° 35'N to 42° 05' N and 80° 04'E to 80° 35'E, covering a
190 drainage area of 1324 km². Elevation ranges from 1600 m to 7100 m a.s.l. with an average
191 value as high as 4100 m a.s.l. Precipitation occurs mainly in summer and rarely in winter, and
192 winter precipitation always comes in the form of snowfall. Snow coverage accumulates in
193 winter and ablates from spring into late summer when it melts away completely; the snow

194 coverage dynamics can be obtained from MODIS data (see Figure 4). The basin is highly
195 glacierized with approximately 33% of the basin area covered by glacier ice (see Figure 1). The
196 glacier coverage stretches from approximately 3000 m to 7100 m a.s.l. and exists mainly at an
197 altitude range of 4000 m to 5000 m a.s.l. Glacier melt and snowmelt form runoff as long as the
198 temperature rises above a certain threshold and provide primary sources for downstream
199 discharge.

200 TRB is a heavily studied mountain watershed in northwestern China. The relevant
201 literature (Kang and Zhu, 1980; Shen *et al.*, 2003; Xie *et al.*, 2004; Gao *et al.*, 2011; Sun *et al.*,
202 2012) are reviewed below, and the main conclusions about the hydrometeorological
203 characteristics are summarized as follows:

204 (1) The climate presents strong altitudinal variability. The mean annual precipitation in
205 higher mountain areas is approximately 1200 mm (Kang *et al.*, 1980), while it is approximately
206 only 180 mm in the outlet plain area (Xie *et al.*, 2004). The mean annual temperature ranges
207 from below 0°C in mountain areas to approximately 9°C at the basin outlet (Sun *et al.*, 2012).

208 (2) Meltwater is the principal source of streamflow. Snow and glacier meltwater account
209 for approximately 63% of the annual runoff (Kang *et al.*, 1980). The contribution of rainwater
210 is relatively lower and occurs mainly in the storm rain period (May to September) (Xie *et al.*,
211 2004). Groundwater baseflow is smaller but dominates the streamflow in the winter (January,
212 February and December), during which either rainfall or melt rarely occur (Kang *et al.*, 1980).

213 (3) The TRB river network is a simple fan system. Given large topographic drop and
214 moderate drainage area, the runoff concentration time is no longer than one day (Xie *et al.*,
215 2004). Melting and falling water can quickly flow into the main channel and reach the basin
216 outlet.

217 **2.2 Data & Preprocessing**

218 The Tailan gauging station (THS, 1602 m a.s.l.) is located the outlet of the watershed,
219 where runoff, precipitation and temperature have been measured since 1957. To collect
220 temperature and precipitation data at higher elevation, two automatic weather stations (AWS,
221 product type TRM-ZS2) were set up in June 2011 (i.e., XT AWS, at 2116 m a.s.l. and TG AWS,
222 at 2381 m a.s.l.). This relatively short record (from July 1, 2011-December 31, 2012) was used
223 to estimate the lapse rate of precipitation and temperature (see below). The Bingtan automatic

224 weather station (BT AWS, at 3950 m a.s.l.) located in an adjacent catchment (Kumalak basin)
 225 was used to validate the estimated temperature lapse rates. A digital elevation model (DEM)
 226 with a spatial resolution of 30 m was provided by the International Scientific & Technical Data
 227 Mirror Site, Computer Network Information Center of the Chinese Academy of Sciences
 228 (<http://www.gscloud.cn>). Remotely sensed snow cover area (SCA) data were downloaded from
 229 the MODIS website; the MOD10A2 and MYD10A2 products were used, both of which have a
 230 spatial resolution of 500m and a temporal resolution of eight-days. Daily snow cover data was
 231 obtained by linear interpolation of the eight-day data. The China Glacier Inventory (CGI) (Shi,
 232 2008) was used to derive glacier coverage in the TRB. In our experience, most of the snow
 233 melts away after the warm summer period and the lowest snow/ice coverage in the year should,
 234 therefore, be roughly equal to the glacier coverage. Based on an analysis of filtered MODIS
 235 SCA (see Sect. 2.2.3), the lowest values of snow/ice coverage in the study period (2003-2012)
 236 are almost the same, which indicates that TRB glacier coverage is relatively stable during the
 237 study period. The DEM, river system, gauging stations and glacier distribution are shown in
 238 Fig.1.

239 2.2.1 Temperature Lapse Rate

240 Altitudinal distribution of temperature can be estimated through the lapse rate (Rango and
 241 Martinec, 1979; Tabony, 1985). According to Aizen *et al.* (2000), rates of temperature decrease
 242 with increasing elevation are quite different in various months, and ignoring this difference may
 243 lead to significant errors in the simulation of snow accumulation and melt. The lapse rate was
 244 therefore estimated for each month. Temperature variations with altitude can be estimated by
 245 the following equation, i.e.:

$$246 \quad T = T_o + T_p \cdot (H - h) \quad (1)$$

247 where, T_o is the temperature value at low altitude (THS in this study), and T_p is the
 248 temperature lapse rate (usually negative), H and h are the elevation values at high and low
 249 positions, i.e., the mean elevation of two AWS and the elevation of THS, respectively. The
 250 values of T_p in different months are obtained by minimizing the error function, i.e.:

$$251 \quad \min : z = \sum (T_i - (T_{oi} + T_p \cdot (H - h)))^2 \quad (2)$$

252 where, i indicates the i^{th} day in the analyzed month, T_i is the observed temperature in AWS,

253 which is the mean value of the TG AWS and XT AWS in this study.

254 The temperature series data from July 1, 2011 to December 31, 2012 at THS, TG AWS
255 and XT AWS were used to estimate the temperature lapse rate. The results (Table1) indicate
256 significant month-to-month variation ranging from $-0.30^{\circ}\text{C } 100 \text{ m}^{-1}$ in December to $-0.86^{\circ}\text{C } 100$
257 m^{-1} in August. To validate the temperature lapse rates, the estimated and observed temperature
258 data at BT AWS were compared (Fig. 2). We also compared the estimated temperature by an
259 annual constant lapse rate ($-0.62^{\circ}\text{C } 100 \text{ m}^{-1}$, a similar value to previous studies, e.g., Tabony
260 (1985) and Tahir *et al.*(2011)). This constant value is optimized by the same method in Eqn. (2)
261 but using all daily temperature measurements. Figure 2 indicates that the monthly lapse rate
262 method performs better than the annual constant rate method at the BT station for all months
263 throughout the year. Further, the temperature curves estimated by monthly lapse rates for April
264 to August match the observed ones rather well. Note that the estimated temperatures tend to
265 underestimate observed ones for the rest of the months, which, however, will not affect the melt
266 runoff significantly due to the general freezing condition during this period.

267 **2.2.2 Precipitation Lapse Rate**

268 Based on the precipitation series measured at THS, the monthly precipitation to annual
269 precipitation ratio (Fig.3) for the study period (2003-2012) indicates that precipitation occurs
270 mainly in May to September. The lapse rate of precipitation was also estimated monthly, and a
271 similar procedure as temperature was applied. The different is that the precipitation analysis
272 was conducted at a weekly rather than daily time step, and the maximum measured precipitation
273 of the two installed AWS was used instead of the mean value. The analyzed period is limited
274 to the storm rain period (May to September). Other months are not included due to the relatively
275 small precipitation amount. The weekly precipitation lapse rates are listed in Table2. Daily
276 precipitation differences between higher and lower altitudes can be estimated as the weekly
277 precipitation lapse multiplied by the ratio of daily precipitation to the corresponding weekly
278 amount in THS. The precipitation lapse rate was not validated against BT AWS because of
279 significant differences in precipitation distribution between the two basins (i.e., Tailan and
280 Kumalak).

281 **2.2.3 Filtering of MODIS Snow Cover Area Data**

282 Snow cover extent was obtained from MODIS products. The MOD10A2 and MYD10A2

283 products were downloaded from the website <http://reverb.echo.nasa.gov>. In total, we obtained
284 460 eight-day images (two tiles, h23v04 and h24v04) from 2003 to 2012 for each product.
285 Given that the accuracy of the MODIS SCA product is affected by cloud coverage to a
286 significant degree, the remotely sensed images should be filtered to avoid the noise from clouds
287 before using it for hydrological modeling (Ackerman *et al.*, 1998). The following three
288 successive steps are adopted to filter the products based on previous reports (Gafurov and
289 Bardossy, 2009; Wang *et al.*, 2009; Lopez-Burgos *et al.*, 2012):

290 (1) Satellite combination: The snow cover products of two satellites, Terra (MOD10A2)
291 and Aqua (MYD10A2) were combined. As long as the value of a pixel is marked as snow in
292 either satellite, the pixel value is marked as snow.

293 (2) Spatial combination: Inspecting the values of the nearest four pixels around one center
294 pixel marked as cloud, if at least three of the four surrounding pixels are marked as snow, the
295 center pixel is modified as snow.

296 (3) Temporal combination: If one pixel is marked as cloud, its values in the previous and
297 following observations are investigated. If both of the two observed values are snow, then the
298 present value of the same pixel is snow.

299 As an example, the filtered results from year 2004-2005 shown in Fig.4 demonstrate a
300 significant reduction in fluctuation of the SCA products. We find that the lowest values of
301 snow/ice coverage in all years (2003-2012) are relatively stable (from 2003 to 2012 are: 35%,
302 34%, 39%, 36%, 37%, 34%, 41%, 35%, 38%, 39%, showing no obvious trend), which is close
303 to the glacier coverage area (33%) derived from the CGI data mentioned in Sect.2.2. As
304 mentioned before, MODIS snow/ice covered area in later summer is mainly composed of
305 glacier coverage when snow has been melt away completely. The filtered results indicate a
306 relatively stable coverage of glacier in TRB.

307 **2.2.4 Altitudinal Cumulative Melt Curve**

308 The daily temperature of each cell in MODIS SCA images can be estimated by a
309 temperature lapse rate based on its elevation and daily temperature measured at THS. As long
310 as the temperature exceeds a specific threshold value for melt (assumed to be 0°C in this study),
311 a given cell was labeled as an active cell in terms of melt. The land cover type for each cell was
312 classified into glacier, snow, and other land cover according to the CGI and MODIS SCA

313 product. To obtain the area covered by snow only, we subtracted the glacier area in CGI from
314 the SCA (a similar procedure can be found in Luo *et al.*, 2013). When a glacier or snow cover
315 cell is active, it is labeled as a melt cell, and the melt area is computed as the number of active
316 cells multiplied by the area of a cell.

317 Organizing the melt area by elevation from low to high and summing the melt area at each
318 elevation, we can get the altitudinal cumulative melt curve, which can be used to describe the
319 spatiotemporal distribution of melt area. The altitudinal cumulative melt curves calculated from
320 2003 to 2012 for all months (Fig.5) show that melt mainly occur from May to September, which
321 coincides with the precipitation period. Snowmelt starts at an elevation of approximately 1650
322 m a.s.l., while glacier melt starts at an elevation of approximately 2950 m a.s.l, which has an
323 important implication for hydrograph partitioning.

324 **3 Methodology**

325 Theoretically, every drop of water in the streamflow comes ultimately from precipitation.
326 Practically, we can consider water sources for runoff generation in mountain areas as mainly
327 consisting of meltwater from snow and glacier, rainwater, and groundwater. Groundwater at the
328 basin scale is recharged by direct infiltration and run-on infiltration of meltwater or rainwater,
329 and it is mainly discharged as baseflow via a subsurface flow path (especially in mountain areas
330 where the large elevation gradient favors baseflow discharge). For the purpose of hydrograph
331 partitioning, we can consider recharge to be a separate water source for streamflow, independent
332 of meltwater and rainwater, which principally forms the baseflow part of a hydrograph. The
333 remaining part of a hydrograph is principally formed by meltwater and rainwater via surface
334 flow path (Blöschl *et al.*, 2013). We develop three indices to indicate the water sources for
335 runoff generation at the daily time scale. The hydrograph is further partitioned into several sub-
336 parts based on the indices values. Each sub-part is dominated by one or more water sources for
337 runoff generation. With the partitioning hydrographic curves, the parameters of hydrological
338 models are correspondingly grouped by runoff sources and calibrated in a stepwise fashion. We
339 use the THREW model coupled with a temperature-index module as an exploratory tool. To
340 better demonstrate usefulness of the proposed methods, only the runoff generation related
341 parameters, which are also significantly sensitive parameters (see Sect.4.6), are calibrated.
342 Other insensitive parameters are fixed at their initial values, specified *a priori* from the literature

343 or by expert knowledge.

344 **3.1 An Index-based Method for Hydrograph Partitioning**

345 In mountain areas, the relative contribution of different runoff water sources to the total
346 streamflow varies throughout the year (Martinec *et al.*, 1982; Dunn and Colohan, 1999; Yang
347 *et al.*, 2007). For the rainwater source, Fig.3 shows that precipitation in TRB presents strong
348 seasonality and primarily concentrates (more than 76%) in the storm rain period from May to
349 September. During the relatively dry period from October to April, mean precipitation gauged
350 at the THS is just 43 mm, while precipitation in the higher mountainous region is mainly
351 snowfall. Therefore, surface runoff induced by rainwater can rarely occur during relative dry
352 period. It is reasonable to assume that the rainwater source can only contribute to the surface
353 runoff part of a hydrograph on the same day during the storm rain period (May to September)
354 except for the baseflow occurring much later.

355 For the meltwater sources, the altitudinal cumulative melt curves (Fig.5) show that the
356 areas experiencing glacier melt and snowmelt change significantly with elevation. Melt of
357 glacier and snow begins at different elevations in different months, i.e., glacier melt can only
358 occur in the areas higher than 2950 m (the lower elevation limit of glacier coverage) while
359 snowmelt can occur in areas higher than 1650 m. It can be deduced that snowmelt generally
360 occurs at lower elevations than glacier melt. Remember that temperature decreases with
361 increase in altitude. There should exist a period of time during which temperature at 1650 m is
362 higher than snowmelt threshold while temperature above 2950 m is lower than glacier threshold
363 and thus snowmelt does occur but glacier melt not.

364 The groundwater source should be a dominant source for the baseflow part of a hydrograph
365 and, of course, it dominates the recession limb of a hydrograph (part of a baseflow partition)
366 when no rainfall or melting occurs.

367 Based on the above physical understanding, we can partition the hydrograph using the
368 following three indices:

369 (1) Date index (D_i): D_i is used to distinguish the dates on which rainfall and thus possible
370 rainwater directly runoff process occurs. For simplicity, in this study we use D_i to
371 distinguish dry period and storm rain period and assume no rainfall runoff in the dry
372 period, i.e.,

373
$$D_i = \begin{cases} 1, & \text{for days in storm rain period from May to September} \\ 0, & \text{for days in relative dry period from October to April} \end{cases} \quad (3)$$

374 (2) Snowmelt index (S_i): S_i indicates whether snowmelt possibly occurs on a given
375 day:

376
$$S_i = \begin{cases} 1, & \text{for days when temperature at altitude 1650 m is higher than } 0^\circ\text{C} \\ 0, & \text{for other days} \end{cases} \quad (4)$$

377 (3) Glacier melt index (G_i): G_i is used to identify days when glacier melt possibly
378 occurs:

379
$$G_i = \begin{cases} 1, & \text{for days when temperature at altitude 2950 m is higher than } 0^\circ\text{C} \\ 0, & \text{for other days} \end{cases} \quad (5)$$

380 The hydrograph is then partitioned according to the three indices by using the following
381 rules:

382
$$Q = \begin{cases} Q_{SB} & \text{for } S_i=0, G_i=0, \text{ and } D_i = 0 \\ Q_{SB} + Q_{SM} & \text{for } S_i=1, G_i=0, \text{ and } D_i = 0 \\ Q_{SB} + Q_{SM} + Q_{GM} & \text{for } S_i=1, G_i=1, \text{ and } D_i = 0 \\ Q_{SB} + Q_{SM} + Q_{GM} + Q_R & \text{for } D_i = 1 \end{cases} \quad (6)$$

383 where, Q is the overall streamflow series, Q_{SB} stands for the baseflow generated by groundwater
384 source, Q_{SM} for snow meltwater runoff, Q_{GM} for glacier meltwater runoff, and Q_R for rainwater
385 directly runoff. The partitioning principles are described as follows:

386 (1) Groundwater is the dominant component ($Q=Q_{SB}$) when both melt and rainwater
387 directly runoff do not occur. This condition is mathematically equivalent to $S_i+G_i+D_i=0$, which
388 requires $S_i=0$, $G_i=0$, and $D_i=0$;

389 (2) Snow meltwater and groundwater are the dominant components ($Q=Q_{SB}+Q_{SM}$) when
390 the temperature is higher than 0°C at 1650 m a.s.l. and lower than 0°C at 2950 m a.s.l.
391 (requires $S_i=1$, $G_i=0$, and $D_i=0$);

392 (3) Snow meltwater and glacier meltwater coupled with groundwater dominate
393 ($Q=Q_{SB}+Q_{SM}+Q_{GM}$) on days when the temperature at 2950 m a.s.l. exceeds 0°C in October to
394 April. This means $G_i=1$, $D_i=0$, and $S_i=1$, noting that S_i must be equal to 1 when $G_i=1$ for the
395 decreasing nature of temperature along altitude;

396 (4) Finally, all sources are mixed ($Q=Q_{SB}+Q_{SM}+Q_{GM}+Q_R$) for other days in the storm rain

397 period (May to September, $D_i=1$). Each category contains days that could be continuous or
398 discontinuous in time and could lie within different weeks due to temporal variability of
399 precipitation and temperature.

400 **3.2 Tsinghua Representative Elementary Watershed Hydrological Model**

401 The Tsinghua Representative Elementary Watershed model (THREW model) used for the
402 hydrological simulation in this study, has been successfully applied in many watersheds in both
403 China and the United States (see Tian *et al.*, 2008, 2012; Li *et al.*, 2012; Liu *et al.*, 2012 etc.),
404 including an application to a high mountainous catchment of Urumqi River basin by Mou *et al.*
405 (2008). The THREW model adopts the REW (Representative Elementary Watershed) approach
406 to conceptualize a watershed, where REW is the sub-catchment unit for hydrological modeling.
407 The study basin was divided into several units (REW) based on a digital elevation model. Sub-
408 catchment units were further divided into a surface and sub-surface layer, each layer containing
409 several sub-zones. The sub-surface layer is composed of two zones: saturated zone and
410 unsaturated zone, and the surface layer consists of six zones: vegetated zone, bare soil zone,
411 snow covered zone, glacier covered zone, sub-stream-network zone, and main channel reach;
412 see Tian *et al.* (2006) for further details.

413 The main runoff generation processes simulated by the THREW model include rainfall
414 surface runoff, groundwater baseflow, snowmelt and glacier melt. Rainfall surface runoff is
415 simulated by a Xin'anjiang module, which adopts a water storage capacity curve to describe
416 non-uniform distribution of water storage capacity of a sub-catchment (Zhao, 1992). The
417 storage capacity curve is determined by two parameters (spatial averaged storage capacity W_M
418 and shape coefficient B). Rainfall surface runoff forms on areas where storage is replete.
419 Replete areas are calculated by the antecedent storage and current rainfall. The saturation excess
420 runoff is computed based on water balance. The remainder of rainfall can infiltrate into soil and
421 become additional contributions to groundwater. Groundwater forms baseflow that is
422 separately calculated by two coefficients (K_A and K_D). K_A and K_D are outflow coefficients of
423 groundwater storage. Their sum determines the flow rate of groundwater baseflow and their
424 ratio (K_D / K_A) dominate the proportion of free groundwater storage. Infiltration and storage
425 should have effects on the calibration of the two parameters. The Xin'anjiang module has been
426 successfully applied to the Qiedeke, Kaidu, Manasi and Kahai basins in Tianshan Mountain by

427 different authors (Jiang, 1987; Yang *et al.*, 1987; Mu and Jiang, 2009), which indicates its
428 applicability in our study area.

429 For the simulation of melt processes in this study, the THREW model was modified to
430 couple with the temperature-index method, given the easy accessibility of air temperature data
431 and generally good model performance of the temperature-index model (Hock, 2003; Singh *et al.*,
432 2000). Snow and glacier melt are simulated using separate degree-day factors (snowmelt
433 degree day factor D_s and glacier melt degree day factor D_g). Glacier melt only occurs in glacier
434 area according to CGI, which remains stable during the study period (2003-2012, see discussion
435 in Sect. 2.2.3). Precipitation in the snow and glacier zone is divided into rainfall and snowfall
436 according to two threshold temperature values (0°C and 2.5°C are adopted in this study
437 according to Wu and Li (2007)), i.e., when temperature is higher than 2.5°C , all precipitation
438 is rainfall, when temperature is lower than 0°C , all precipitation is snowfall, and when
439 temperature falls between the two thresholds, precipitation is divided into rainfall and snowfall
440 half by half (a simple division scheme adopted here). Rainfall on glacier areas forms runoff and
441 flows into the stream-network directly without infiltration into soil. Snow water equivalent
442 (SWE) on glacier areas is updated by combining snowfall and snowmelt, and for simplicity,
443 snow is assumed to cover all glacier areas when the corresponding SWE is not zero. Snowmelt
444 in glacier areas is simulated using snow degree-day factor D_s until it melts away completely.
445 Snow cover area in non-glacier area is updated using MODIS data. To be noted, snowfall in
446 each subcatchment is calculated according to the daily precipitation and temperature. And
447 snowmelt is simulated using the degree-day method. However, the snow water equivalent in
448 the snow cover zone (non-glacier area) is not computed. The existing of snow cover in each
449 subcatchment is only determined by MODIS snow image. When the MODIS image indicates
450 the existing of snow cover and meanwhile the daily temperature is higher than 0°C , then
451 snowmelt will occur, otherwise, snowmelt will not occur. The identification of snow cover by
452 MODIS image is in accordance with the fact that the partitioning of snowmelt dominant
453 hydrograph is based on MODIS snow products. If the existing of snow cover is determined by
454 snow water equivalent, the temperature parameters to calculate snowfall can have significant
455 effects on the estimation of the degree-day factor for snowmelt. To partly reduce this effect, we
456 calibrate the degree-day factor for snowmelt on the basis of MODIS snow cover products.

457 Although in this way, the water balance of snow cover is not taken into account in the snow
458 cover zone, it should not impact the calibration of the degree-day factor for snowmelt. Since
459 MODIS SCA products (i.e., MYD10A2) are available from 2003, the model simulation period
460 is from 2003 to 2012, of which 2003-2007 for calibration and 2008-2012 for evaluation. The
461 time step for simulation is daily.

462 **3.3 Stepwise Calibration of Grouped Parameters Upon Partitioning Curves**

463 Model parameters are grouped *a priori* according to their connection with causal physical
464 mechanisms (see Table 3). According to Xie *et al.* (2004) and Kang *et al.* (1980), parameters
465 that control groundwater baseflow, snowmelt, glacier melt, and rainwater surface runoff should
466 be the most sensitive parameters for the runoff simulation (also see our sensitivity analysis in
467 Sect. 4.6). These parameters are subjected to calibration in this study. They are related to the
468 corresponding hydrograph parts and then calibrated in a stepwise manner: first, groundwater
469 baseflow parameters (K_A and K_D) are estimated based on the Q_{SB} part of the hydrograph. Second,
470 snowmelt degree day factor (D_s) is calibrated upon the $Q_{SB}+Q_{SM}$ part. Third, glacier melt
471 degree-day factor (D_g) is determined according to the $Q_{SB}+Q_{SM}+Q_{GM}$ part. Finally, rainfall
472 surface runoff parameters (B , W_M) are calibrated on days when D_i equals to 1, i.e., the
473 $Q_{SB}+Q_{SM}+Q_{GM}+Q_R$ part of hydrograph.

474 In each step, only the specific parameter group is subjected to calibration. The parameters
475 determined in the previous steps are kept constant, and all other parameters that will be
476 calibrated in the next steps adopt their initial values. As the simulation in each step can, to some
477 degree, be affected by the initial conditions produced in the preceding step, an iterative
478 procedure is implemented to progressively minimize this influence. The parameter groups are
479 first calibrated based on the corresponding hydrograph parts, and then the stepwise sequence is
480 repeated until the calibrated parameters converge, i.e., the difference in parameter values
481 between two contiguous iterations is less than 10%. In each calibration step, we use $RMSE_{ln}$
482 (Eqn. (7), emphasizing low flow) or $RMSE$ (Eqn. (8), emphasizing high flow) as objective
483 function for parameter optimization. The remaining, insensitive, parameters are determined *a*
484 *priori* according to previous modeling experience (mainly from Sun *et al.* (2012)) and listed in
485 Table 3. The initial values of the calibrated parameters are also determined *a priori* according
486 to Sun *et al.* (2012) and Tian *et al.* (2012).

487 The overall streamflow can be simulated with all calibrated parameters, which is evaluated
 488 with NSE and $NSE \ln$ (logarithm Nash Criterion) values. Given that it is relatively easier to
 489 obtain high evaluation merit values in snowmelt driven basins due to strong seasonality of
 490 streamflow, we further adopt a simple benchmark model (the inter-annual mean value for every
 491 calendar day) to evaluate performance of the proposed method by subtracting streamflow
 492 seasonality. This benchmark model is proposed by Schaeffli and Gupta (2007) for basins having
 493 a relatively constant seasonality. The improvement of a model comparing to the benchmark
 494 model is quantified by the BE , see Eqn. (9) for detail.

$$495 \quad RMSE \ln = \sqrt{\frac{1}{n} \sum_{i=1}^n (\log Q_{obs}(i) - \log Q_{sim}(i))^2} \quad (7)$$

$$496 \quad RMSE = \sqrt{\frac{1}{n} \sum_{i=1}^n (Q_{obs}(i) - Q_{sim}(i))^2} \quad (8)$$

$$497 \quad BE = 1 - \frac{\sum_{i=1}^n (Q_{obs}(i) - Q_{sim}(i))^2}{\sum_{i=1}^n (Q_{obs}(i) - Q_{ben}(i))^2} \quad (9)$$

498 4 Results and Discussion

499 4.1 Partitioning Hydrographic Curves

500 The hydrograph from 2003 to 2012 was partitioned based on Eqn. (6). In total, we obtained
 501 four kinds of partitioning curves, i.e. Q_{SB} part, $Q_{SB}+Q_{SM}$ part, $Q_{SB}+Q_{SM}+Q_{GM}$ part and
 502 $Q_{SB}+Q_{SM}+Q_{GM}+Q_R$ part. As an example, the partitioning curves in 2003 are shown in Fig. 6, in
 503 which the melting period ranges from late February to late November (labeled as red and green
 504 dots). Snowmelt (red dots) starts in February and ends in November, while glacier melt (green
 505 dots) starts later (March) and stops earlier (October). This melt situation agrees well with the
 506 previous studies of Kang *et al.* (1980) and Sun *et al.* (2012). Hydrograph parts dominated by
 507 groundwater source mainly fall into December, January and February and are denoted by black
 508 dots. The rainwater surface runoff occurs in the storm rain period only (May to September,
 509 denoted by blue dots). The total number of days of $Q_{SB}+Q_{SM}$ part from 2003 to 2007 is 365,
 510 and that of $Q_{SB}+Q_{SM}+Q_{GM}$ part is 249, while the $Q_{SB}+Q_{SM}+Q_{GM}+Q_R$ part occupies 765 days.
 511 The numbers of non-melt days (i.e. the Q_{SB} part, due to glacier melt generally occurs in the
 512 $Q_{SB}+Q_{SM}+Q_{GM}+Q_R$ part) in the five years are 114, 80, 89, 96, and 68, respectively.

513 Correspondingly, the mean temperatures in those years gauged at the THS are 8.9, 10.1, 9.9,
514 10.4, and 11.3°C, respectively. A lower mean annual temperature causes a longer non-melt
515 period in that year and vice versa. Note that the partitioning curves can be discontinuous in time
516 due to the spatial-temporal variability of temperature.

517 **4.2 Model Calibration by the Stepwise Method**

518 The six key parameters (K_A , K_D , D_s , D_g , W_M , and B) were firstly calibrated by the proposed
519 stepwise and iterative method. To focus on baseflow generated by the groundwater source
520 during the Q_{SB} period, the $RMSEln$ metric that emphasizes low flow is chosen as the evaluation
521 criterion for the calibration of parameters K_A and K_D . Conversely, high flow is our focus for
522 the remaining periods ($Q_{SB}+Q_{SM}$, $Q_{SB}+Q_{SM}+Q_{GM}$, $Q_{SB}+Q_{SM}+Q_{GM}+Q_R$) and the $RMSE$ metric is
523 chosen as the evaluation criterion for calibration of parameters D_s , D_g , and W_M and B . To deal
524 with interaction between steps, an iterative calibration approach was adopted. A total of five
525 iterations was implemented until the parameter estimates became stable; the simulation of each
526 kind of partitioning curve in each step of the last iteration is presented in Fig. 7. The calibrated
527 parameters are shown in Table 4 and the evaluation merits are listed in Table 5.

528 Figure 7a shows that the magnitude of baseflow in Q_{SB} part was captured well at most of
529 the times. The $RMSEln$ merit is 0.302 m³/s, and the parameters K_A and K_D were determined as
530 1.1 and 0.002 respectively. Streamflow in the $Q_{SB}+Q_{SM}$ part is dominated by both snow
531 meltwater and groundwater. The Fig.7b shows that melt peak flow events have also been
532 captured well by a calibrated D_s as 2.5 mm °C⁻¹ day⁻¹ after the determination of K_A and K_D in
533 the first step. For the $Q_{SB}+Q_{SM}+Q_{GM}$ part, glacier meltwater began to control the streamflow in
534 combination with snow meltwater and groundwater. Snowmelt and baseflow were determined
535 *a priori* by previously calibrated parameters. The remaining residual between the simulated and
536 observed discharge can be attributed to glacier melt alone, which was thus used for the
537 calibration of glacier melt factor D_g . The $RMSE$ value for this hydrograph partition was
538 optimized as 4.784 m³/s and we obtained a sound simulation by a calibrated D_g as 7.2 mm °C⁻¹
539 day⁻¹ as shown in Fig.7c. During the storm rain periods ($Q_{SB}+Q_{SM}+Q_{GM} +Q_R$ part), rainwater
540 directly runoff is an additional important component of river runoff. Similarly, parameters W_M
541 and B can be calibrated separately after *a priori* determination of melt runoff and groundwater
542 baseflow. The simulated $RMSE$ value in this period is 12.650 m³/s, with calibrated $W_M=10.50$ cm

543 and $B=0.80$. The overall daily streamflow simulation is obtained by combining the four
544 partitions together (see Figure 8a). The corresponding NSE index is 0.881 and $NSEln$ is 0.929.
545 Generally the results suggest a sound simulation compared to the observation.

546 To be noted, the calibrated values of melt degree day factors D_s ($2.5\text{mm } ^\circ\text{C}^{-1} \text{ day}^{-1}$) and D_g
547 ($7.2\text{mm } ^\circ\text{C}^{-1} \text{ day}^{-1}$) are similar to the values obtained in other studies in Tainshan area, e.g., D_s
548 is calibrated as $2.5 \text{ mm } ^\circ\text{C}^{-1} \text{ day}^{-1}$ by Liu *et al.* (2012), and D_s and D_g are estimated as $3.1 \text{ mm } ^\circ\text{C}^{-1}$
549 day^{-1} and $7.3 \text{ mm } ^\circ\text{C}^{-1} \text{ day}^{-1}$ respectively based on observed mass balance data by Liu *et al.*
550 (1999), which indicates the robustness of our calibration method.

551 4.3 Comparison to Automatic Calibration Method

552 For comparison, we also carry out an automatic calibration with the help of the ε -NSGAI
553 algorithm, an optimization method developed by Deb *et al.* (2002) and Kollat and Reed (2006).
554 The six parameters were calibrated together and evaluated by NSE value of the overall
555 hydrograph. The run time of the automatic algorithm is about 5 weeks (840 hour on a desktop
556 equipped with an Intel Core i7 CPU with 2.8GHz). The NSE value for the final optimized
557 parameters is 0.868, and the $NSEln$ value is 0.846 (Fig. 8b), both of which are lower than the
558 values obtained by the proposed stepwise method. The parameters calibrated by ε -NSGAI are
559 listed in Table 4, and are different from those calibrated by the stepwise method. Specifically,
560 the snowmelt degree-day factor (D_s) and groundwater baseflow parameters (K_A and K_D)
561 obtained by ε -NSGAI are $2.03\text{mm } ^\circ\text{C}^{-1} \text{ day}^{-1}$ and 5.6 and 99.1 respectively. The evaluation
562 merits of $RMSE$ and $RMSEln$ for each partitioning curve are also shown in Table 5. In general,
563 the simulation by the automatic algorithm is not as good as that by the stepwise method,
564 especially for the low and middle flow partitions ($Q_{SB}+Q_{SM}$ and $Q_{SB}+Q_{SM}+Q_{GM}$). This may be
565 due to the tendency of NSE-based automatic calibration to emphasize high flows.

566 To make a further evaluation, a benchmark model suggested by Schaepli and Gupta (2007)
567 is used for the comparison, which simply simulates daily runoff as the inter-annual daily mean
568 value. Simulation results by the benchmark model are shown in the Figure 8c, which shows
569 NSE value as 0.815 and $NSEln$ value as 0.923. The high NSE and $NSEln$ values can be attributed
570 to the strong seasonality of stream discharge in the study basin (Schaepli and Gupta, 2007). The
571 BE index (Eqn. (9), see Table 5) is used to measure the improvement of simulations by the
572 calibration methods compared to the benchmark model. A positive value for BE means that the

573 evaluated method outperforms the benchmark model. Figure 8 shows the simulations of daily
574 streamflow by the three methods (Fig.8a by stepwise calibration method, Fig.8b by automatic
575 calibration method and Fig.8c by benchmark model), which shows better simulation by the two
576 calibration runs with THREW model than the benchmark model (*BE* values are both positive).
577 The stepwise calibration run obtained a *BE* value of 0.355, while *BE* of the automatic calibration
578 run is 0.271. The benchmark model describes the mean value of daily discharge on each
579 calendar day. The higher the *BE* value is, the better the seasonal variability of the hydrograph
580 is captured by the evaluation method. The higher *BE* value in the stepwise calibration method
581 can be attributed to the better simulation of middle and low flows which are dominated by
582 groundwater and melt water (Fig.8a). However, *BE* values simulated by two calibrated
583 parameter sets are both relatively low, which is attributed to the poor mimic of the (rapidly
584 rising and falling) peaks.

585 Note that the automatic calibration method based on *NSE* value of the overall hydrograph
586 adopts 1D measurement information to optimize four parameter groups. Benefitting from the
587 partitioning curves, however, the stepwise calibration method increases the dimension of
588 hydrological signature to four. The signature dimension is now equal to the number of
589 parameter groups, and the grouped parameters can be optimized according to their
590 corresponding runoff sources separately. A sound simulation of the overall hydrograph is
591 obtained by the reasonable reproduction of the separate partitioning curves. Therefore,
592 parameters calibrated by the stepwise method are inclined to have more explicit physical basis.

593 In regards to computation efficiency, the stepwise calibration required 385 runs of the
594 model to complete, with each model run taking about 1.5 minutes and the total computation
595 time being about 10 hrs. In contrast, the state-of-the-art automatic calibration algorithm
596 required about 5 weeks of CPU time consumption on a desktop equipped with an Intel Core i7
597 CPU and 2.8GHz. The comparison indicates that the stepwise calibration method is both more
598 physically based as well as more computationally efficient.

599 It is worth noting, the performance of the automatic calibration algorithm can increase if
600 the algorithm keeps on running, and even be higher than that of the step-wise calibration method.
601 The comparison here is intending to show that the step-wise calibration method based on
602 hydrograph partition can achieve considerable performance more effectively. The automatic

603 algorithm here treats all the parameters equally during the calibration period. Each parameter
604 should be optimized when searching for the optimal parameter set. This searching algorithm
605 hampers the efficiency of the calibration procedure without identifying the dominant sub-
606 periods for different parameters. In the step-wise calibration method, only parameters that are
607 responsible for the simulation of corresponding hydrograph partition are optimized in each step.
608 And also the calibration of parameter by this method reflects the role of each parameter for the
609 basin runoff generation.

610 **4.4 Evaluation for the Stepwise Calibration Method**

611 The parameter set calibrated by the stepwise method is applied to the evaluation period
612 (2008~2012), and the daily discharge simulation is shown in Fig.9a. The evaluation merits are
613 listed in Table 5. The *NSE*, *NSEln* and *RMSE* values for the whole period indicate sound
614 evaluation results but general lower performance compared to calibration period. However, the
615 evaluation results by the stepwise method are still significant better than the benchmark model,
616 which obtained a *NSE* value as low as 0.577 (Fig. 9b and Table 5). The *BE* value in evaluation
617 period by the stepwise calibration method is 0.413. Furthermore, from the partition perspective,
618 the *RMSEln* and *RMSE* values for four partitions in Table 5 show that the low flow simulations
619 (Q_{SB} , $Q_{SB}+Q_{SM}$, and $Q_{SB}+Q_{SM}+Q_{GM}$ parts) are pretty good and even outperform the calibration
620 simulations. The high flow simulation ($Q_{SB}+Q_{SM}+Q_{GM}+Q_R$ part) is, however, insufficient, with
621 *RMSE* 16.727m³/s (compared to 12.65 m³/s in calibration period). The lower performance of
622 overall evaluation should be attributed to the insufficiency in storm rain days, especially for
623 some extreme storm events in the summer of 2010 (see Fig. 9a). The underestimation of these
624 events is likely due to inadequate observations of rainfall, which are principally due to the
625 strong spatial variability of rainfall in mountainous areas. It is widely acknowledged that the
626 extreme runoff events are difficult to capture in mountain area, where gauged station is scarce,
627 on the daily scale (Aizen *et al.*, 2000; Jasper *et al.*, 2002). However, the accuracy of our results
628 is similar to Li and Williams (2008) (used SRM model) and Liu *et al.*(2012) (who used the
629 MIKE-SHE model) who performed similar work in a basin that is close to TRB in Tianshan
630 Mountains. Their Nash values for daily discharge varied from 0.51 to 0.78, and also failed to
631 simulate the peak flows in summer. They also attributed the low efficiency to the heavy
632 precipitation.

633 To further evaluate the robustness of the stepwise calibration method based on partitioning
634 curves, cross validation was implemented. The hydrograph in the evaluation period was
635 partitioned based on dominant runoff sources, as was done in the calibration years 2003-2007.
636 We calibrated the model to 2008-2012 and evaluated it for 2003-2007. The new calibrated
637 parameter values are $K_A=0.9$, $K_D=0.003$, $D_s=2.2 \text{ mm } ^\circ\text{C}^{-1} \text{ day}^{-1}$, $D_g=7.4 \text{ mm } ^\circ\text{C}^{-1} \text{ day}^{-1}$,
638 $W_M=10.2\text{cm}$ and $B=0.77$, which are similar to the values calibrated in 2003-2007 listed in Table
639 4. The *NSE*, *NSEln* and *RMSE* values for calibration period 2008-2012 and evaluation period
640 2003-2007 are 0.757, 0.900, 10.892m³/s and 0.883, 0.910, 8.589m³/s, respectively, using this
641 new calibrated parameter set. The simulations of the two periods by cross validation are
642 presented in Fig.9c-d, which shows similar performance by two calibrated parameter sets and
643 further demonstrates the robustness of the proposed stepwise calibration method.

644 **4.5 Sensitivity Analysis on Index-based Partitioning Method**

645 The stepwise calibration method relies heavily on the hydrograph partition for different
646 runoff sources. The indices defined in Sect. 3.1 are keys to identify the dominant days for melt
647 water and rainwater. The definitions for elevation bands for the 0 °C Isotherm and for storm rain
648 days in the year producing rainwater runoff should have significant influence on the parameter
649 calibration. In this study, the elevation band of 0 °C Isotherm for snowmelt is fixed and defined
650 as 1650m. This value should have minimal effect on the snowmelt simulation, as the occurrence
651 of snowmelt is actually determined by the MODIS snow cover data. Glacier cover area is
652 assumed as constant, which is very rough for we have only one CGI data. In this section, we
653 define different elevation bands of 0 °C Isotherm for glacier to analyze the effect of glacier area
654 variation on the model calibration. We also select different seasons as the storm rain period to
655 analyze its sensitive effect.

656 According to the CGI data, the glacier area extends from the altitude of 2950m in 2002.
657 Considering the possible variability, we define four different lowest elevation bands for the
658 glacier area (LEG), i.e., -500m (2450m), -200m (2750m), +200m (3150m) and +500m (3450m).
659 As an example, various hydrograph partition patterns in year 2003 are shown in Fig. 10. For
660 the storm rain period (SRP), new seasons are defined as April to October, April to September,
661 May to October, and June to August compared to the benchmark period May to September. A
662 new hydrograph partition pattern in year 2003 is also shown in Fig. 10. The left column in Fig.

663 10 shows that the $Q_{SB}+Q_{SM}+Q_{GM}$ partition becomes longer while the $Q_{SB}+Q_{SM}$ partition
664 becomes shorter when the LEG is lower. Therefore, glacier melt starts earlier and ends later in
665 the years with lower LEG. In the right column, the $Q_{SB}+Q_{SM}+Q_{GM}$ partition becomes longer
666 with the shorter SRP, while the variation of the $Q_{SB}+Q_{SM}$ partition can be negligible. Parameters
667 were re-calibrated according to the new partition curves, and the results are shown in Table 6,
668 indicating the increase of degree-day factor for glacier melt (D_g) with the increase of the LEG.
669 The value of D_g is also found to become higher when the SRP falls in the warmer months. The
670 variation of LEG imposes significant impacts on the calibration of D_g , with a result ranging
671 from 5.8 to 8.0mm °C⁻¹ day⁻¹, while the variation of SRP principally impacts the calibration of
672 parameter W_M , with a result ranging from 8.2 to 10.5cm. However, the *NSE* values (see Table
673 6) for different settings show minimal differences. This can be attributed to the fact that
674 parameters are optimized on separate partitioning curves in the stepwise calibration method.
675 Each hydrograph partition can be well simulated by adjusting the parameter values. The
676 partition patterns can influence the value of parameters significantly but only slightly influence
677 the discharge simulation. Among various LEGs, the setting of 2950m leads to the highest *NSE*
678 value. Glacier melt degree day factor (D_g) calibrated with this LEG is 7.2 mm °C⁻¹ day⁻¹, which
679 is very close to the value estimated as 7.3 mm °C⁻¹ day⁻¹ by Liu *et al.*(1999), in which the D_g is
680 estimated according to the observed glacier mass balance data in Tianshan area. This can further
681 demonstrate the reasonability of the assumption in Sect. 3.2 that the glacier area is stable and
682 its lowest elevation is fixed at 2950m during the study period. For the various storm rain periods
683 (SRP), when the May to October period is adopted, the discharge simulation is slightly better
684 than the benchmark setting of SRP, i.e. May to September. This phenomenon seems to indicate
685 the importance of precipitation measurement as discussed in Sect. 4.4. With the help of more
686 advanced precipitation measurement, the storm rain period can be determined more precisely
687 to improve the model simulation.

688 To evaluate the relative dominance of multiple runoff sources on the total runoff, we
689 compute their contributions to total runoff by various LEG and SRP in Fig.11. The mean
690 contributions of every runoff source are as follows: groundwater contributes 17%, snow
691 meltwater contributes 16.5%, glacier meltwater contributes 40% and rainwater directly runoff
692 contributes 26.5%. Total melt water (snowmelt and glacier melt) occupies approximately 56.5%

693 and is close to the ratio 63% suggested by Kang *et al.* (1980).

694 **4.6 Sensitivity Analysis on Parameters**

695 The number of parameters to be calibrated is determined by the parameter sensitivity and
696 *a priori* analysis. To evaluate the effect of different parameters on the simulation of different
697 hydrograph partitions, we implemented a simple parameter sensitivity procedure that is carried
698 out by a “one-at-a-time” approach. Parameters from different groups in Table 3 are selected for
699 sensitivity analysis, including saturated hydraulic conductivity for u-zone K_s^u , saturated
700 hydraulic conductivity for s-zone K_s^s , subsurface flow coefficient K_A and K_D , manning
701 roughness coefficient for hillslope n^l , spatial heterogeneous coefficient for infiltration capacity
702 α^{FL} , ground surface depression storage capacity $Fmax^b$, shape coefficient to calculate the
703 saturation excess runoff area from the Xin’anjiang model B , spatial averaged tension water
704 storage capacity in the Xin’anjiang model W_M , glacier degree day factor D_g and snowmelt
705 degree per day factor D_s . Parameter are varied from -50% to +50% of the calibrated values
706 using the stepwise method in Table 4. The relative change (R_{MS}) of simulated measure merits
707 ($RMSE_{ln}$ or $RMSE$) for different hydrograph partitions are used to evaluate the sensitivity (Eqn.
708 (10)), where MS is the value of measure merits by the calibrated parameter, MS_+ is the merits
709 value obtained by the parameter +50% of the calibrated one, and MS_- is the merits value
710 obtained by the parameter -50% of the calibrated one. The sensitivity simulation results are
711 shown in Table 7, which demonstrates the dominant control of parameter K_A , K_D , W_M , B , D_s and
712 D_g . Some parameters have significant effects on simulation of multi hydrograph partitions. For
713 example, parameters controlling the $Q_{SB}+Q_{SM}+Q_{GM}+Q_R$ period can also have significant effect
714 on the other periods. To minimize this interaction, iterative calibration was implemented in the
715 calibration procedure. The number of calibrated parameters is determined as six, which control
716 the main runoff sources (i.e. groundwater baseflow, snowmelt, glacier melt and rainwater
717 directly runoff). Note that the low dimension of parameter calibration should not account for
718 the low efficiency of peak flow simulation, referring to the similar study in Tianshan mountain
719 areas by Li and Williams (2008), and Liu *et al.*(2012), in which the models have a higher
720 parameter dimension (higher than six), and the peak flow simulations are still inadequate.

$$721 \quad R_{MS} = \left| \frac{MS_+ - MS_-}{MS} \right| \times 100\% \quad (10)$$

722 **5 Summary and Conclusion**

723 This study proposes diagnostic calibration approach to extracting hydrological signatures
724 from available data series in a mountain area, which can be further used to partition the
725 hydrograph into dominant runoff sources. The parameters of a hydrological model were
726 grouped according to runoff sources and then related to the corresponding hydrologic
727 partitioning curve. Each parameter group was calibrated to improve the simulation of the
728 corresponding partitioning curve in a stepwise way. In this way, the dimension of hydrological
729 signature is expanded to equal the number of parameter groups. The parameter uncertainty due
730 to interaction of parameters is reduced via an iterative calibration procedure. Application to a
731 mountain watershed in the Tianshan Mountain in northwestern China showed that the approach
732 performed reasonably well. Cross validation and comparison to an automatic calibration
733 method indicated its applicability.

734 Note that a semi-distributed hydrological model was utilized to illustrate the proposed
735 diagnostic calibration approach in the high mountainous Tailan River Basin. Glacier mass
736 balance is not simulated in the model and the glacier coverage was kept fixed during the study
737 period, which can be subject to significant change in the context of global warming. According
738 to existing studies (Stahl *et al.*, 2008; Schaefli and Huss, 2011; Jost *et al.*, 2012), glacier mass
739 balance data is useful to constrain the parameter uncertainty for hydrological modeling in a
740 glaciated basin. While arguing that our assumption of unchanged glacier coverage will not
741 weaken the importance of the proposed approach, we acknowledge that an improved model
742 coupled with glacier mass balance equations will improve the accuracy of hydrological
743 simulation aided by glacier mass balance observations. This is left for future research.

744 A prerequisite for the proposed approach is hydrograph partitioning based on dominant
745 runoff sources. The key to the partition procedure is to identify the functional domain of each
746 runoff source from signature information extracted from easily available data. A partition can
747 be achieved in which the relative roles of different runoff sources in the basin runoff vary
748 significantly with time. The mountain watershed is an area in which the runoff sources can be
749 separated by the combination of topography, ground-gauged temperature and precipitation, and
750 remotely sensed snow and glacier coverage. Other areas with strong temporal variability of
751 catchment wetness along with precipitation (e.g., monsoon zones) could also be suitable for the

752 proposed approach. The Dunne runoff is prone to dominate the hydrograph when the catchment
753 is wet and it could switch to Hortonian runoff rapidly under the combination of high evaporative
754 demand and less precipitation, as shown by Tian *et al.* (2012) in the Blue River basin of
755 Oklahoma. This is, however, also left for future research.

756 *Acknowledgments.* We wish to thank Mr. Wang Xinhui for his assistance in collecting
757 hydrometeorology data in the Tailan River basin, and thank Charlie Luce and Viviana Lopez-
758 Burgos who provided great help in MODIS snow coverage product filtering. The authors would
759 also like to thank sincerely two Referees (B. Schafli and M. Zappa) and Editor Markus Weiler
760 for his careful comments, which improve the quality of manuscript significantly. This study
761 was supported by the National Science Foundation of China (NSFC 51190092, U1202232,
762 51222901) and the foundation of the State Key Laboratory of Hydroscience and Engineering
763 of Tsinghua University (2012-KY-03, 2014-KY-01). Their support is greatly appreciated.

764 **References**

- 765 Ackerman, S. A., Strabala, K. I., Menzel, W. P., Frey, R. A., Moeller, C. C. and Gumley, L. E.:
766 Discriminating clear sky from clouds with MODIS, *J. Geophys. Res.*,103, 32141-32157,
767 1998.
- 768 Aizen, V., Aizen, E., Glazirin, G. and Loaiciga, H. A.: Simulation of daily runoff in Central
769 Asian alpine watersheds, *J. Hydrol.*, 238, 15-34, 2000.
- 770 Akyurek, Z., Surer, S. and Beser, O.: Investigation of the snow-cover dynamics in the Upper
771 Euphrates Basin of Turkey using remotely sensed snow-cover products and
772 hydrometeorological data, *Hydrol. Process.*,25 (23), 3637-3648, 2011.
- 773 Arnold, J. G. and Allen, P. M.: Automated methods for estimating baseflow and ground water
774 recharge from streamflow records, *Journal of the American Water Resources Association*,
775 35, 411-424, 1999.
- 776 Arnold, J. G., Allen, P. M., Muttiah, R. and Bernhardt, G.: Automated base-flow separation and
777 recession analysis techniques, *Ground Water*, 33, 1010-1018, 1995.
- 778 Beven, K.: Prophecy, reality and uncertainty in distributed hydrological modelling, *Adv. Water*
779 *Resour.*, 16, 41-51, 1993.
- 780 Beven, K.: Equifinality and uncertainty in geomorphological modelling, *The Scientific Nature*
781 *of Geomorphology: Proceedings of the 27th Binghamton Symposium in Geomorphology*,
782 289-313, 1996.
- 783 Beven, K. and Binley, A.: The future of distributed models-model calibration and uncertainty
784 prediction, *Hydrol. Process.*, 6, 279-298, 1992.
- 785 Beven, K. and Freer, J.: Equifinality, data assimilation, and uncertainty estimation in
786 mechanistic modelling of complex environmental systems using the GLUE methodology, *J.*
787 *Hydrol.*,249, 11-29, 2001.
- 788 Blöschl, G., Sivapalan, M., Wagener, T., Viglione, A. and Savenije, H.(Eds.): *Runoff*
789 *Prediction in Ungauged Basins: Synthesis Across Processes, Places and Scales*, Cambridge
790 *Univ. Press*, New York,2013.
- 791 Boyle, D. P., Gupta, H. V. and Sorooshian, S.: Toward improved calibration of hydrologic
792 models: Combining the strengths of manual and automatic methods, *Water Resour. Res.*, 36,
793 3663-3674, 2000.
- 794 Brazil, L.: Multilevel calibration strategy for complex hydrologic simulation models, NOAA
795 *Technical Report*, NWS 42, Fort Collins, 217 pp, 1989.
- 796 Bulygina, N., McIntyre, N. and Wheeler, H.: Conditioning rainfall-runoff model parameters for
797 ungauged catchments and land management impacts analysis, *Hydrol. Earth Syst. Sci.*, 13
798 (6), 893-904, 2009.
- 799 Daly, S. F., Davis, R., Ochs, E. and Pangburn, T.: An approach to spatially distributed snow
800 modelling of the Sacramento and San Joaquin basins, California, *Hydrol. Process*, 14 (18SI),
801 3257-3271, 2000.
- 802 Deb, K., Pratap, A., Agarwal, S. and Meyarivan, T.: A fast and elitist multiobjective genetic
803 algorithm: NSGA-II, *IEEE Transactions on evolutionary computation*, 6, 182-197, 2002.
- 804 Detenbeck, N. E., Brady, V. J., Taylor, D. L., Snarski, V. M. and Batterman, S. L.: Relationship
805 of stream flow regime in the western Lake Superior basin to watershed type characteristics,
806 *J. Hydrol.*, 309, 258-276, 2005.
- 807 Duan, Q., Sorooshian, S. and Gupta, V.: Effective and efficient global optimization for

808 conceptual rainfall-runoff models, *Water Resour. Res.*, 28, 1015-1031, 1992.

809 Dunn, S. M. and Colohan, R. J. E.: Developing the snow component of a distributed
810 hydrological model: a step-wise approach based on multi-objective analysis, *J. Hydrol.*, 223,
811 1-16, 1999.

812 Eder, G., Fuchs, M., Nachtnebel, H. and Loibl, W.: Semi-distributed modelling of the monthly
813 water balance in an alpine catchment, *Hydrol. Process.*, 19, 2339-2360, 2005.

814 Farmer, D., Sivapalan, M. and Jothityangkoon, C.: Climate, soil, and vegetation controls upon
815 the variability of water balance in temperate and semiarid landscapes: Downward approach
816 to water balance analysis, *Water Resour. Res.*, 39, 1035, 2003.

817 Fierz, C., Ribet, P., Adams, E., Curran, A., Fohn, P., Lehning, M. and Pluss, C.: Evaluation of
818 snow-surface energy balance models in alpine terrain, *J. Hydrol.*, 282 (1-4), 76-94, 2003.

819 Gafurov, A. and Bardossy, A.: Cloud removal methodology from MODIS snow cover product,
820 *Hydrol. Earth Syst. Sci.*, 13, 1361-1373, 2009.

821 Gan, T. Y. and Biftu, G. F.: Automatic calibration of conceptual rainfall-runoff models:
822 Optimization algorithms, catchment conditions, and model structure, *Water Resour. Res.*, 32,
823 3513-3524, 1996.

824 Gao, W., Li, Z. and Zhang, M.: Study on Particle-size Properties of Suspended Load in Glacier
825 Runoff from the Tomor Peak, *Arid Zone Research*, 28, 449-454, 2011(in Chinese).

826 Gomez-Landesa, E. and Rango, A.: Operational snowmelt runoff forecasting in the Spanish
827 Pyrenees using the snowmelt runoff model, *Hydrol. Process.*, 16, 1583-1591, 2002.

828 Gupta, H. V., Kling, H., Yilmaz, K. K. and Martinez, G. F.: Decomposition of the mean squared
829 error and NSE performance criteria: Implications for improving hydrological modelling, *J.*
830 *Hydrol.*, 377, 80-91, 2009.

831 Gupta, H. V., Sorooshian, S. and Yapo, P. O.: Toward improved calibration of hydrologic
832 models: Multiple and noncommensurable measures of information, *Water Resour. Res.*, 34,
833 751-763, 1998.

834 Gupta, V. K. and Sorooshian, S.: Uniqueness and observability of conceptual rainfall-runoff
835 model parameters: The percolation process examined, *Water Resour. Res.*, 19, 269-276,
836 1983.

837 Gupta, V. K. and Sorooshian, S.: The Automatic Calibration of Conceptual Catchment Models
838 Using Derivative-Based Optimization Algorithms, *Water Resour. Res.*, 21, 437-485, 1985.

839 Gupta, H. V., Wagener, T. and Liu, Y.: Reconciling theory with observations: elements of a
840 diagnostic approach to model evaluation, *Hydrol. Process.*, 22, 3802-3813, 2008.

841 Gurtz, J., Baltensweiler, A. and Lang, H.: Spatially distributed hydrotope-based modelling of
842 evapotranspiration and runoff in mountainous basins, *Hydrol. Process.*, 13, 2751-2768, 1999.

843 Haberlandt, U., Klocking, B., Krysanova, V. and Becker, A.: Regionalisation of the base flow
844 index from dynamically simulated flow components - a case study in the Elbe River Basin,
845 *J. Hydrol.*, 248, 35-53, 2001.

846 Hingray, B., Schaepli, B., Mezghani, A. and Hamdi, Y.: Signature-based model calibration for
847 hydrological prediction in mesoscale Alpine catchments, *Hydrolog. Sci. J.*, 55 (6), 1002-
848 1016, 2010.

849 Hock, R.: Temperature index melt modelling in mountain areas, *J. Hydrol.*, 282, 104-115, 2003.

850 Hooper, R. P. and Shoemaker, C. A.: A Comparison of Chemical and Isotopic Hydrograph
851 Separation, *Water Resour. Res.*, 22, 1444-1454, 1986.

852 Howard, C.: Revisiting the degree-day method for snowmelt computations – Discussion, *Water*
853 *Resources Bulletin*, 32 (2), 411-413, 1996.

854 Huss, M., Farinotti, D., Bauder, A. and Funk, M.: Modelling runoff from highly glacierized
855 alpine drainage basins in a changing climate, *Hydrol. Process.*, 22 (19SI), 3888-3902, 2008.

856 Jasper, K., Gurtz, J. and Herbert, L.: Advanced flood forecasting in Alpine watersheds by
857 coupling meteorological observations and forecasts with a distributed hydrological model, *J.*
858 *Hydrol.*,267 (1-2),40-52, 2002.

859 Jiang, H. F.: Snow ablation modeling and its application to Qiedeke basin, *Journal of Xinjiang*
860 *Agricultural University*, 1, 67-75, 1987 (in Chinese).

861 Johnston, P. R. and Pilgrim, D. H.: Parameter optimization for watershed models, *Water Resour.*
862 *Res.*, 12, 477-486, 1976.

863 Jost, G., Moore, R. D., Menounos, B. and Wheate, R.: Quantifying the contribution of glacier
864 runoff to streamflow in the upper Columbia River Basin, Canada, *Hydrol. Earth Syst.*
865 *Sci.*,16,849-860,2012.

866 Jothityangkoon, C., Sivapalan, M. and Farmer, D. L.: Process controls of water balance
867 variability in a large semi-arid catchment: downward approach to hydrological model
868 development, *J. Hydrol.*, 254, 174-198, 2001.

869 Juston, J., Seibert, J. and Johansson, P.: Temporal sampling strategies and uncertainty in
870 calibrating a conceptual hydrological model for a small boreal catchment, *Hydrol.*
871 *Process.*,23 (21), 3093-3109, 2009.

872 Kane, D. L., Gieck, R. E., and Hinzman, L. D.: Snow Modeling at Small Alaskan Arctic
873 Watershed, *Journal of Hydrologic Engineering*, 2 (4), 204-210, 1997.

874 Kang, E., Zhu, S. and Huang, M.: Some Results of the Research on Glacial Hydrology in the
875 Region of MT. Tuomuer, *Journal of Glaciology and Geocryology*, 2, 18-21, 1980(in
876 Chinese).

877 Klok, E. J., Jasper, K., Roelofsma, K. P., Gurtz, J. and Badoux, A.: Distributed hydrological
878 modelling of a heavily glaciated Alpine river basin, *Hydrolog. Sci. J.*,46 (4), 553-570, 2001.

879 Kollat, J. B. and Reed, P. M.: Comparing state-of-the-art evolutionary multi-objective
880 algorithms for long-term groundwater monitoring design, *Adv. Water Resour.*, 29, 792-807,
881 2006.

882 Li, H. Y., Sivapalan, M. and Tian, F. Q.: Comparative diagnostic analysis of runoff generation
883 processes in Oklahoma DMIP2 basins: The Blue River and the Illinois River, *J. Hydrol.*, 418,
884 90-109, 2012.

885 Li, X. G. and Williams M. W.: Snowmelt runoff modelling in an arid mountain watershed,
886 Tarim Basin, China, *Hydrol. Process.*,22 (19SI), 3931-3940, 2008.

887 Liu, D. F., Tian, F. Q., Hu, H. C. and Hu, H. P.: The role of run-on for overland flow and the
888 characteristics of runoff generation in the Loess Plateau, China, *Hydrolog. Sci. J.*, 57, 1107-
889 1117, 2012.

890 Liu, S. Y., Xie, Z. C., Wang, N. L. and Ye, B. S.: Mass balance sensitivity to climate change:
891 a case study of glacier no. 1 at Urumqi riverhead, Tianshan mountains, China, *Chin. Geogr.*
892 *Sci.*, 9, 134-140, 1999.

893 Liu, T., Willems, P., Feng, X. W., Li, Q., Huang, Y., Bao, A. M., Chen, X., Veroustraete, F.
894 and Dong, Q. H.: On the usefulness of remote sensing input data for spatially distributed
895 hydrological modelling: case of the Tarim River basin in China, *Hydrol. Process.*,26 (3),

896 335-344, 2012.

897 Lopez-Burgos, V., Gupta, H. V. and Clark, M.: A probability of snow approach to removing
898 cloud cover from MODIS Snow Cover Area products, *Hydrol. Earth Syst. Sci. Discuss*, 9,
899 13693-13728, 2012.

900 Luo, Y., Arnold, J., Liu, S., Wang, X. and Chen, X.: Inclusion of glacier processes for
901 distributed hydrological modeling at basin scale with application to a watershed in Tianshan
902 Mountains, northwest China, *J. Hydrol.*, 477, 72-85, 2013.

903 Martinec, J., Oeschger, H., Schotterer, U. and Siegenthaler, U.: Snowmelt and groundwater
904 storage in alpine basin, In *Hydrological Aspects of Alpine and High Mountain Areas*,
905 Wallingford, United Kingdom: IAHS Press, 169–175, 1982.

906 McCuen, R. H.: *Hydrologic analysis and design*, Prentice Hall, New Jersey pp.355-360, 1989.

907 Mendoza, G. F., Steenhuis, T. S., Walter, M. T. and Parlange, J. Y.: Estimating basin-wide
908 hydraulic parameters of a semi-arid mountainous watershed by recession-flow analysis, *J.*
909 *Hydrol.*, 279, 57-69, 2003.

910 Mou, L., Tian, F., Hu, H. and Sivapalan, M.: Extension of the Representative Elementary
911 Watershed approach for cold regions: constitutive relationships and an application, *Hydrol.*
912 *Earth Syst. Sci.*, 12, 565-585, 2008.

913 Mu, Z. X. and Jiang, H. F.: Establishment of snowmelt type Xin'anjiang watershed model based
914 on digital elevation model, *Journal of Xinjiang Agricultural University*, 5 (32), 75-80, 2009
915 (in Chinese).

916 Nash, J. E. and Sutcliffe, J. V.: River flow forecasting through conceptual models part I — A
917 discussion of principles, *J. Hydrol.*, 10, 282-290, 1970.

918 Nathan, R. J., McMahon, T. A.: Evaluation of automated techniques for base flow and recession
919 analyses, *Water Resour. Res.*, 26, 1465-1473, 1990.

920 Nejadhashemi, A. P., Shirmohammadi, A., Sheridan, J. M., Montas, H. J. and Mankin, K. R.:
921 Case Study: Evaluation of Streamflow Partitioning Methods, *J. Irrig. Drain. Eng.*, 135, 791-
922 801, 2009.

923 Pellicciotti, F., Brock, B., Strasser, U., Burlando, P., Funk, M. and Corripio, J.: An enhanced
924 temperature-index glacier melt model including the shortwave radiation balance:
925 development and testing for Haut Glacier d'Arrolla, Switzerland, *Journal of Glaciology*, 51
926 (175), 573-587, 2005.

927 Pinder, G. F. and Jones, J. F.: Determination of the ground-water component of peak
928 Determination of the ground-water component of peak discharge from the chemistry of total
929 runoff, *Water Resour. Res.*, 5, 438-445, 1969.

930 Rango, A. and Martinec, J.: Application of a Snowmelt-runoff Model Using Landsat Data, *Nord.*
931 *Hydrol.*, 10, 225-238, 1979.

932 Richter, B. D., Baumgartner, J. V., Powell, J. and Braun, D. P.: A method for assessing
933 hydrologic alteration within ecosystems, *Conservation Biology*, 10, 1163-1174, 1996.

934 Schaefli, B. and Gupta, H. V.: Do Nash values have value, *Hydro. Process.*, 21 (15), 2075-2080,
935 2007.

936 Schaefli, B., Hingray, B., Niggli, M. and Musy, A.: A conceptual glacio-hydrological model
937 for high mountainous catchments, *Hydrol. Earth Syst. Sci.*, 9 (1-2), 95-109, 2005.

938 Schaefli, B. and Huss, M.: Integrating point glacier mass balance observations into hydrologic
939 model identification, *Hydrol. Earth Syst. Sci.*, 15, 1227-1241, 2011.

940 Shamir, E., Imam, B., Gupta, H. V. and Sorooshian, S.: Application of temporal streamflow
941 descriptors in hydrologic model parameter estimation, *Water Resour. Res.*, 41, W06021,
942 doi:10.1029/2004WR003409, 2005a.

943 Shamir, E., Imam, B., Morin, E., Gupta, H. V. and Sorooshian, S.: The role of hydrograph
944 indices in parameter estimation of rainfall-runoff models, *Hydrol. Process.*, 19, 2187-2207,
945 2005b.

946 Shen, Y., Liu, S., Ding, Y. and Wang, S.: Glacier Mass Balance Change in Tailanhe River
947 Watersheds on the South Slope of the Tianshan Mountains and its impact on water resources,
948 *Journal of Glaciology and Geocryology*, 25, 124-129, 2003(in Chinese).

949 Shi, Y.: *Concise Glacier Inventory of China*, Shanghai Popular Science Press., Shanghai, China,
950 2008(in Chinese).

951 Singh, P., Kumar, N. and Arora, M.: Degree-day factors for snow and ice for Dokriani Glacier,
952 Garhwal Himalayas, *J. Hydrol*, 235, 1-11, 2000.

953 Sivapalan, M., Bloschl, G., Zhang, L. and Vertessy, R.: Downward approach to hydrological
954 prediction, *Hydrol. Process.*, 17, 2101-2111, 2003.

955 Sorooshian, S. and Gupta, V. K.: Automatic calibration of conceptual rainfall-runoff models-
956 the question of parameter observability and uniqueness, *Water Resour. Res.*, 19, 260-268,
957 1983.

958 Spear, R. C. and Hornberger, G. M.: Eutrophication in peel inlet—II. Identification of critical
959 uncertainties via generalized sensitivity analysis, *Water Research*, 14, 43-49, 1980.

960 Stahl, K., Moore, R. D., Shea, J. M., Hutchinson, D. and Cannon, A. J.: Coupled modelling of
961 glacier and streamflow response to future climate scenarios, *Water Resour. Res.*, 44, 2008.

962 Sun, M., Yao, X., Li, Z. and Li, J.: Estimation of Tailan River Discharge in the Tianshan
963 Mountains in the 21st Century, *Advances on Climate Change Research*, 8, 342-349, 2012(in
964 Chinese).

965 Swamy, A. N. and Brivio, P. A.: Modelling runoff using optical satellite remote sensing data
966 in a high mountainous alpine catchment of Italy, *Hydrol. Process.*, 11 (11), 1475-1491, 1997.

967 Tabony, R. C.: The variation of surface temperature with altitude, *Meteorological Magazine*,
968 114, 37-48, 1985.

969 Tahir, A. A., Chevallier, P., Arnaud, Y., Neppel, L. and Ahmad, B.: Modeling snowmelt-runoff
970 under climate scenarios in the Hunza River basin, Karakoram Range, Northern Pakistan, *J.*
971 *Hydrol*, 409, 104-117, 2011.

972 Tian, F. Q., Hu, H. P. and Lei, Z. D.: Thermodynamic watershed hydrological model:
973 Constitutive relationship, *Science in China, Ser. E-Technological Sciences*, 51, 1353-1369,
974 2008.

975 Tian, F., Hu, H., Lei, Z. and Sivapalan, M.: Extension of the Representative Elementary
976 Watershed approach for cold regions, *Hydrol. Earth Syst. Sci.*, 10, 619-644, 2006.

977 Tian, F. Q., Li, H. Y. and Sivapalan, M.: Model diagnostic analysis of seasonal switching of
978 runoff generation mechanisms in the Blue River basin, Oklahoma, *J. Hydrol*, 418, 136-149,
979 2012.

980 Van Griensven, A. and Bauwens, W.: Multiobjective autocalibration for semidistributed water
981 quality models, *Water Resour. Res.*, 39, 1348, 2003.

982 Van Straten, G. T. and Keesman, K. J.: Uncertainty propagation and speculation in projective
983 forecasts of environmental change: A lake-eutrophication example, *J. Forecast.*, 10, 163-190,

984 1991.

985 Vivoni, E. R., Entekhabi, D., Bras, R. L. and Ivanov, V. Y.: Controls on runoff generation and
986 scale-dependence in a distributed hydrologic model, *Hydrol. Earth Syst. Sci.*, 11, 1683-1701,
987 2007.

988 Vrugt, J. A., Gupta, H. V., Bastidas, L. A., Bouten, W. and Sorooshian, S.: Effective and
989 efficient algorithm for multiobjective optimization of hydrologic models, *Water Resour. Res.*,
990 39, 1214, 2003a.

991 Vrugt, J. A., Gupta, H. V., Bouten, W. and Sorooshian, S.: A Shuffled Complex Evolution
992 Metropolis Algorithm for Optimization and Uncertainty Assessment of Hydrological Model
993 Parameters, *Water Resour. Res.*, 39, 1201, doi:10.1029/2002WR001642, 8., 2003b.

994 Wang, X. W., Xie, H. J., Liang, T. G. and Huang, X. D.: Comparison and validation of MODIS
995 standard and new combination of Terra and Aqua snow cover products in northern Xinjiang,
996 China, *Hydrol. Process.*,23, 419-429, 2009.

997 Westerberg, I. K., Guerrero, J. L., Younger, P. M., Beven, K. J., Seibert, J., Halldin, S., Freer,
998 J. E. and Xu, C. Y.: Calibration of hydrological models using flow-duration curves, *Hydrol.*
999 *Earth Syst. Sci.*,15 (7), 2205-2227, 2011.

1000 Wu, J., L. L.:A rain-on-snow mixed flood forecast model and its application, *Engineering*
1001 *Journal of Wuhan University*,40,20-23,2007(in Chinese).

1002 Xie, C., Ding, Y., Liu, S. and Han, H.: Analysis on the Glacial Hydrological Features of the
1003 Glaciers on the South Slope of Mt. Tuomuer and the Effects on Runoff, *Arid Land*
1004 *Geography*, 27, 570-575, 2004(in Chinese).

1005 Yadav, M., Wagener, T. and Gupta, H.: Regionalization of constraints on expected watershed
1006 response behavior for improved predictions in ungauged basins, *Adv. Water Resour*, 30,
1007 1756-1774, 2007.

1008 Yang, D. Q., Zhao, Y. Y., Armstrong, R., Robinson, D. and Brodzik, M. J.: Streamflow
1009 response to seasonal snow cover mass changes over large Siberian watersheds, *J. Geophys.*
1010 *Res.*, 112, F02S22F2, 2007.

1011 Yang, X. S., Jiang, H. F., Huang, C. R. Zheng, Z., and Yong, G.: An applied study on the
1012 snowmelt type of Xin'anjiang watershed model at the Kaidu river basin, *Journal of Xinjiang*
1013 *Agricultural University*,4, 82-90, 1987 (in Chinese).

1014 Yilmaz, K. K., Gupta, H. V. and Wagener, T.: A process-based diagnostic approach to model
1015 evaluation: Application to the NWS distributed hydrologic model, *Water Resour. Res.*,
1016 44,W09417, doi:10.1029/2007WR006716, 2008.

1017 Zhang, Z. X., Wagener, T., Reed, P. and Bhushan, R.: Reducing uncertainty in predictions in
1018 ungauged basins by combining hydrologic indices regionalization and multiobjective
1019 optimization, *Water Resour. Res.*, 44 (W00B04), doi:10.1029/2008WR006833, 2008.

1020 Zhao, R. J.: The Xin'anjiang model applied in China, *J. Hydrol*,135,371-381,1992.

1021

Table1. Estimated monthly temperature lapse rate in the TRB

Month	Temperature lapse rate ($^{\circ}\text{C}/\text{day}/100\text{ m}$)
January	-0.38
February	-0.38
March	-0.66
April	-0.76
May	-0.80
June	-0.78
July	-0.82
August	-0.86
September	-0.66
October	-0.60
November	-0.54
December	-0.30
Annual	-0.62

1022

1023

Table 2. Estimated week-precipitation lapse rate in storm rain months

Month	Precipitation lapse rate (mm/week/ 100 m)
May	1.63
June	1.69
July	3.14
August	2.40
September	2.28

1024

1025
1026

Table 3. Grouped parameters in the THREW model. Parameters subjected to calibration are highlighted in red.

Category	Symbol	Unit	Description	Value
Subsurface	K_s^u	m s ⁻¹	Saturated hydraulic conductivity for u-zone	1.25E-05
	K_s^s	m s ⁻¹	Saturated hydraulic conductivity for s-zone	1.25E-05
	K_A	-	Coefficient used to calculate subsurface flow	Calibrated
	K_D	-	Coefficient used to calculate subsurface flow	Calibrated
Routing	n^t	-	Manning roughness coefficient for hillslope, obtained from the literature according to land use and vegetation type	1.50E-01
	n^r	-	Similar to n^t , roughness coefficient for channel	3.00E-01
Infiltration	α^{EFL}	-	Spatial heterogeneous coefficient for exfiltration capacity	1.00E+00
	α^{IFL}	-	Spatial heterogeneous coefficient for infiltration capacity	1.50E+00
Interception	$F \max^b$	m	Ground surface depression storage capacity	0.00E+00
	α^{vb}	m	Maximum rainfall depth a single leaf can intercept and hold	1.00E-05
Rainfall runoff	B	-	Shape coefficient to calculate the saturation excess runoff area from the Xin'anjiang model	Calibrated
	W_M	cm	Spatial averaged tension water storage capacity in the Xin'anjiang model	Calibrated
Melt	D_g	mm °C ⁻¹ day ⁻¹	Glacier melt degree day factor	Calibrated
	D_s	mm °C ⁻¹ day ⁻¹	Snowmelt degree day factor	Calibrated

1027

1028

Table 4. Calibrated parameters by the stepwise and automatic methods

Parameter	Stepwise Calibrated	Automatic Calibrated
K_A	1.1	5.6
K_D	0.002	99.1
$D_s(\text{mm } ^\circ\text{C}^{-1} \text{ day}^{-1})$	2.5	2.03
$D_g(\text{mm } ^\circ\text{C}^{-1} \text{ day}^{-1})$	7.2	7.52
$W_M(\text{cm})$	10.5	11.9
B	0.80	0.62

1029

Table 5. Evaluation merits for the stepwise and automatic calibration methods

Merits	Calibration period	Calibration period	Calibration period	Evaluation period	Evaluation period
	Automatic method	Stepwise method	Benchmark model	Stepwise method	Benchmark model
$RMSEln(Q_{SB}, m^3/s)$	0.352	0.302	-	0.213	-
$RMSE(Q_{SB}+Q_{SM}, m^3/s)$	2.807	1.811	-	1.762	-
$RMSE(Q_{SB}+Q_{SM}+Q_{GM}, m^3/s)$	6.079	4.784	-	4.558	-
$RMSE(Q_{SB}+Q_{SM}+Q_{GM}+Q_R, m^3/s)$	13.245	12.650	-	16.727	-
NSE	0.867	0.881	0.815	0.752	0.577
$NSEln$	0.841	0.929	0.923	0.894	0.844
$RMSE (m^3/s)$	8.990	8.459	10.534	11.021	14.381
BE	0.271	0.355	-	0.413	-

1032 Table 6. Sensitive analysis of the calibrated parameters on lowest elevation band for glacier
 1033 area (LEG) and storm rain period (SRP). *NSE* is the Nash Sutcliffe Efficiency value for the
 1034 calibration period.

	LEG(a.s.l. m)	$D_s(\text{mm/d/}^\circ\text{C})$	$D_g(\text{mm/d/}^\circ\text{C})$	$W_M(\text{cm})$	B	K_A	K_D	NSE
	3450	2.2	8.0	10.1	0.70	0.7	0.002	0.870
	3150	2.5	7.9	10.1	0.75	0.7	0.002	0.871
SRP:	2950	2.5	7.2	10.5	0.80	1.1	0.002	0.881
May. To Sep.	2750	3.0	6.8	10.2	0.75	1.0	0.002	0.880
	2450	2.8	5.8	10.0	0.78	0.8	0.002	0.876
	SRP	$D_s(\text{mm/d/}^\circ\text{C})$	$D_g(\text{mm/d/}^\circ\text{C})$	$W_M(\text{cm})$	B	K_A	K_D	NSE
	Jun. to Aug.	2.9	7.5	8.2	0.75	0.9	0.002	0.871
	May. to Oct.	2.8	6.9	9.4	0.76	0.8	0.002	0.882
LEG=2950m	May. to Sep.	2.5	7.2	10.5	0.80	1.1	0.002	0.881
	Apr. to Sep.	2.2	7.1	8.3	0.75	0.9	0.002	0.878
	Apr. to Oct.	2.6	6.9	9.4	0.77	1.1	0.002	0.881

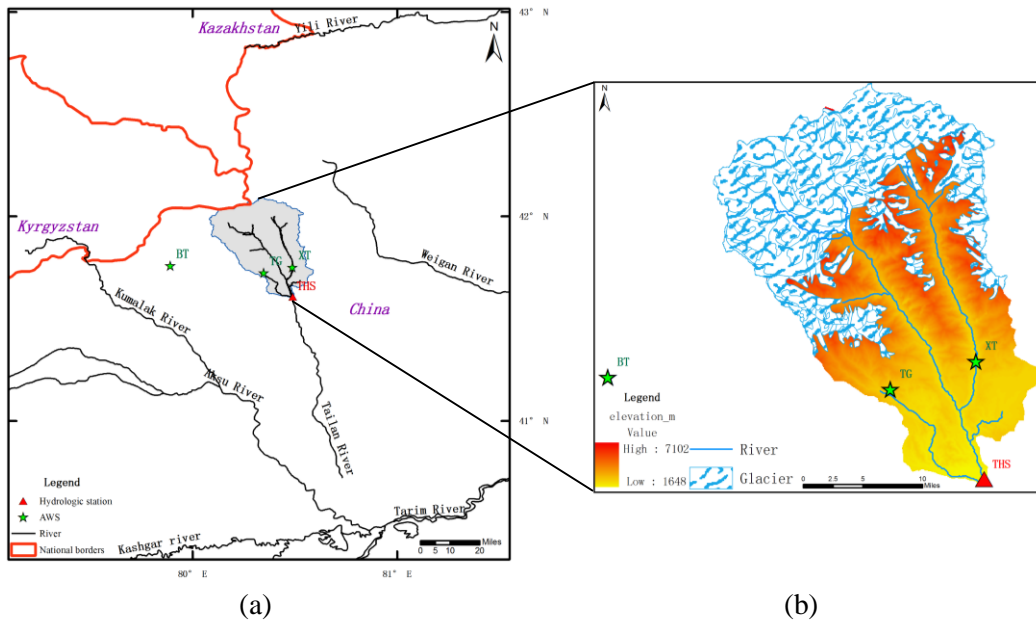
1035

1036
1037

Table 7. R_{MS} (%) for parameter sensitivity (R_{MS} values indicating the most sensitive parameters are labeled in bold and red)

Merits	Subsurface				Routing	Infiltration	Interception	Rainfall Runoff		Melt	
	K_s^u	K_s^s	K_A	K_D	n^t	α^{IFL}	$F \max^b$	W_M	B	D_s	D_g
$RMSE_{ln}$ (Q_{SB})	9.70	11.14	38.44	44.39	15.70	0.12	0.08	1.07	18.51	7.53	2.88
$RMSE$ ($Q_{SB}+Q_{SM}$)	0.32	0.40	11.91	0.06	9.35	0.47	0.14	8.27	25.14	51.22	0.69
$RMSE$ ($Q_{SB}+Q_{SM}+Q_{GM}$)	0.22	0.21	0.62	0.64	10.00	0.17	0.25	7.92	0.29	26.28	40.79
$RMSE$ ($Q_{SB}+Q_{SM}+Q_{GM}+Q_R$)	0.17	0.85	0.57	0.97	1.84	0.08	0.06	19.35	22.48	10.78	11.57

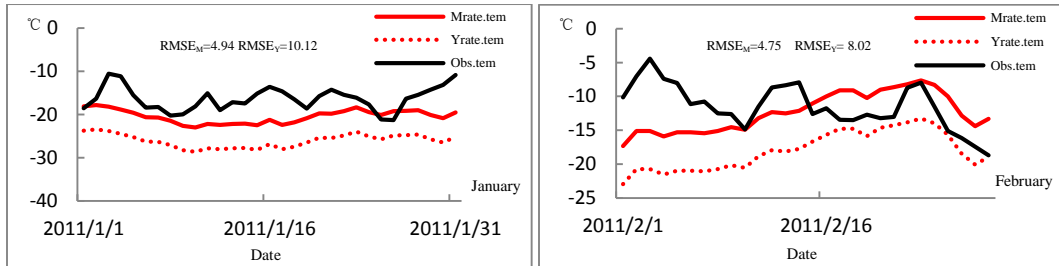
1038



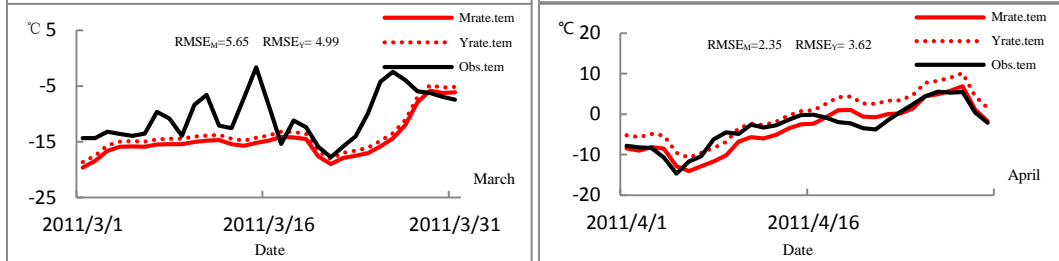
1039
 1040
 1041
 1042
 1043
 1044
 1045
 1046
 1047

Figure 1. Location of the Tailan River basin in Xinjiang Uygur Autonomous Region, China. Two automatic weather stations (TG at 2381 m a.s.l. and XT at 2116 m a.s.l.) were set up in upstream mountain area in July, 2011. Additionally, the BT weather station (3950 m a.s.l.) located in the adjacent Kumalak River basin was used to validate the estimated temperature lapse rates. The Tailan Hydrologic Station (THS) has gauged streamflow data at the catchment outlet since 1957(a). Glacier occupies approximately 33% of the total basin area (b).

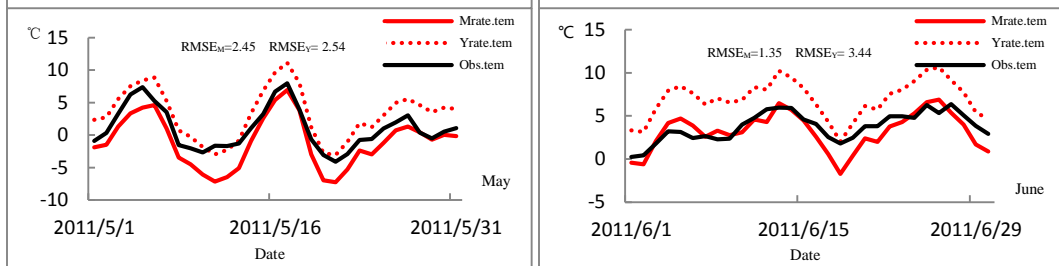
1048



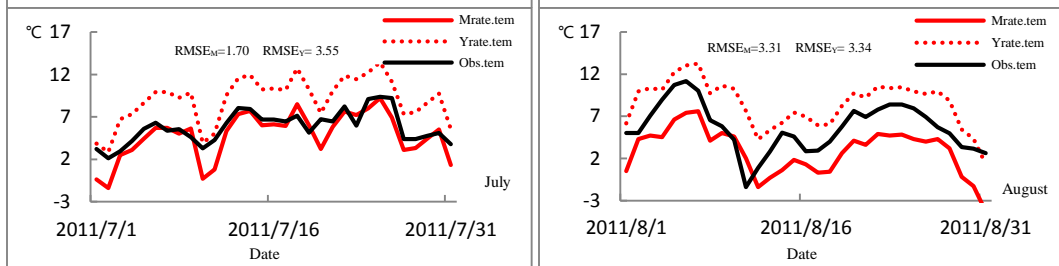
1049



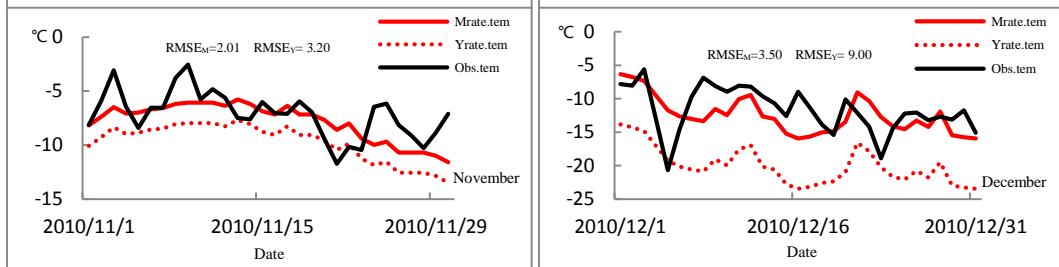
1050



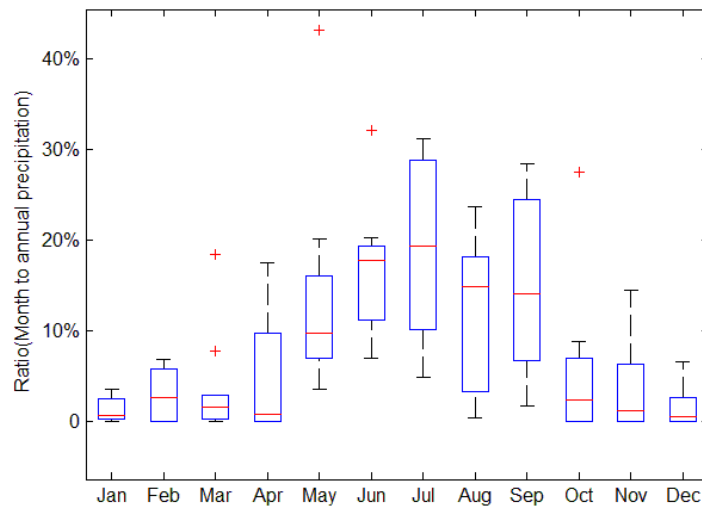
1051



1052

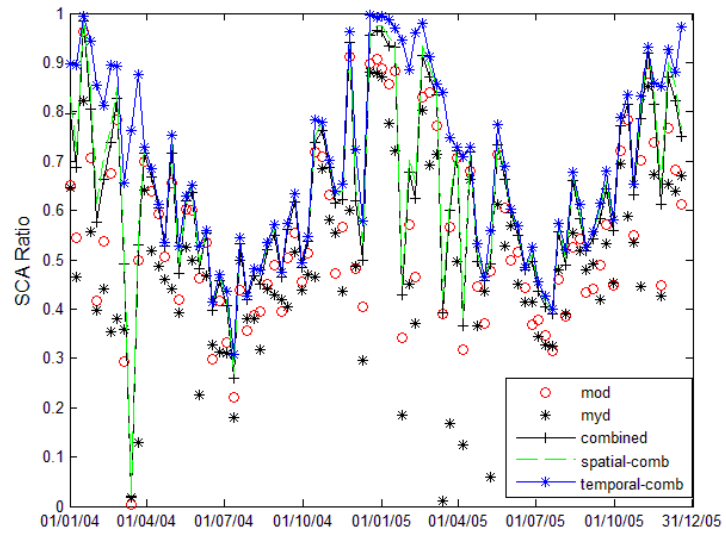


1053 Figure 2. Evaluation of the estimated temperature lapse rate at the BT station. The black solid
 1054 line is the observed temperature series at BT (Obs.tem); the red solid line is the estimated
 1055 temperature by monthly lapse rate (Mrate.tem).The red dotted line indicates the estimated
 1056 temperature based on annual constant rate (Yrate.tem). The goodness of fit between the
 1057 observed and estimated temperature is measured by $RMSE_M$ for monthly lapse rate and
 1058 $RMSE_Y$ for annual constant rate, respectively. The temperature series in September and
 1059 October are absent at BT.



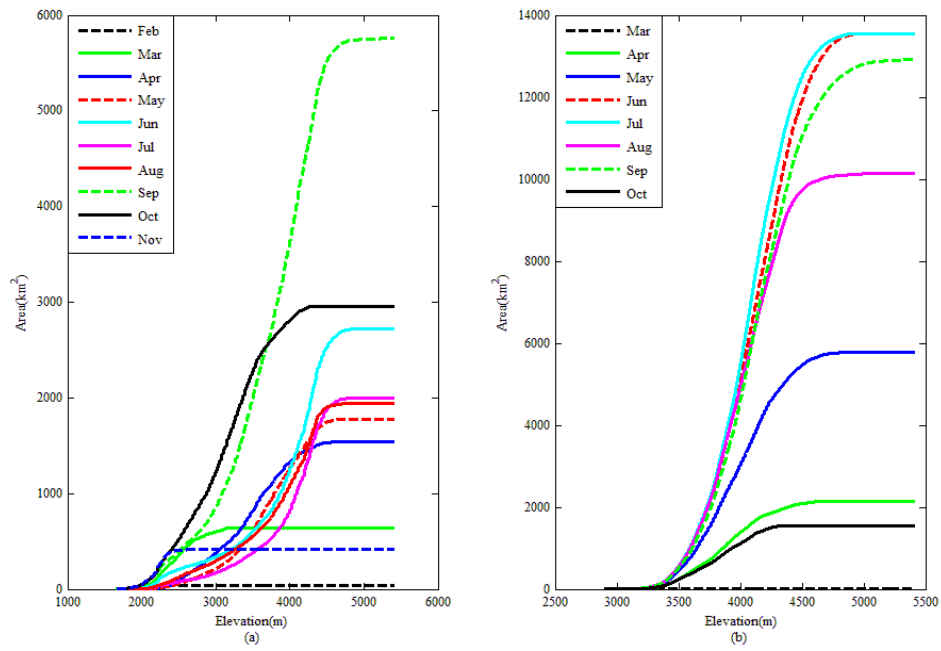
1060

1061 Figure 3. Proportion of monthly precipitation to annual amount (2003~2012). The red line in
 1062 each box represents the median value for each month from 2003 to 2012. Red crosses indicate
 1063 abnormal values that exceed 1.5 times the inter quartile range.



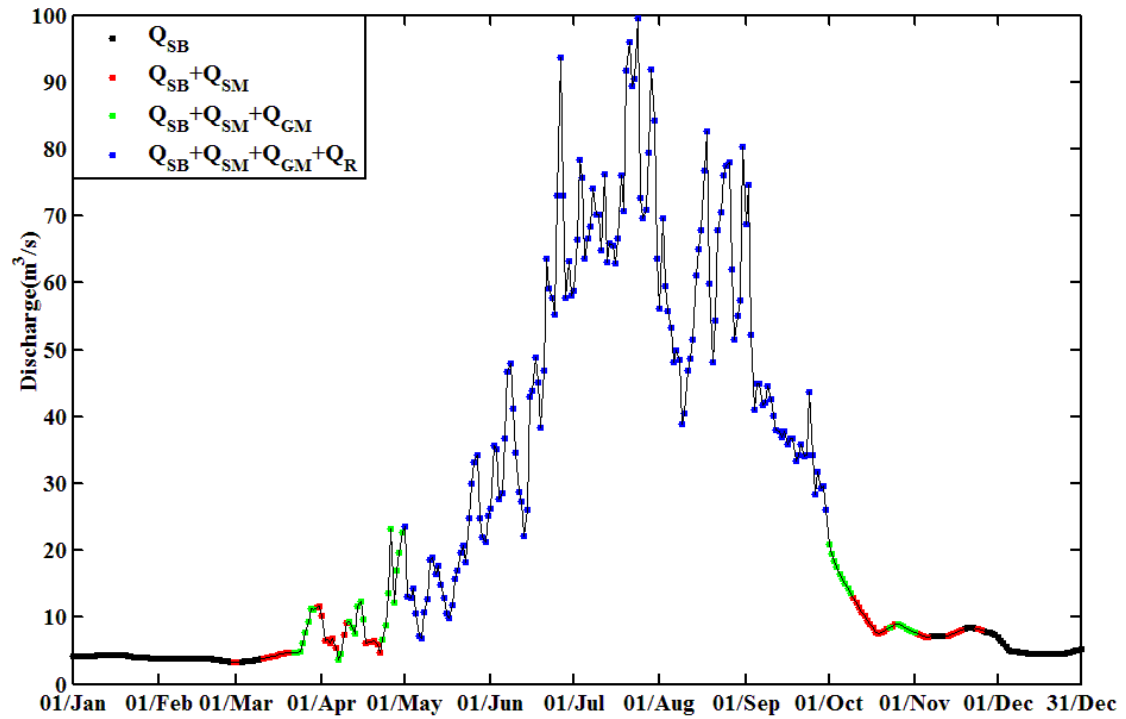
1064
 1065
 1066
 1067
 1068

Figure 4. Filtered MODIS eight-day snow-cover products (2004-2005). The term ‘mod’ is the snow cover area from MOD10A2 products, ‘myd’ is MYD10A2 products, ‘combined’ is the combined result from step1, ‘spatial-comb’ from step2 and ‘temporal-comb’ from step3. See Sect. 2.2.3 for details.



1069
 1070
 1071
 1072
 1073
 1074

Figure 5. Altitudinal Cumulative Melt Curve. (a) Cumulative monthly snowmelt area distribution by elevation (2003~2012). (b) Cumulative monthly glacier melt area distribution by elevation (2003~2012). The snowmelt areas in December and January and the glacier melt areas in November, December, January and February are zero and are not shown in this figure.



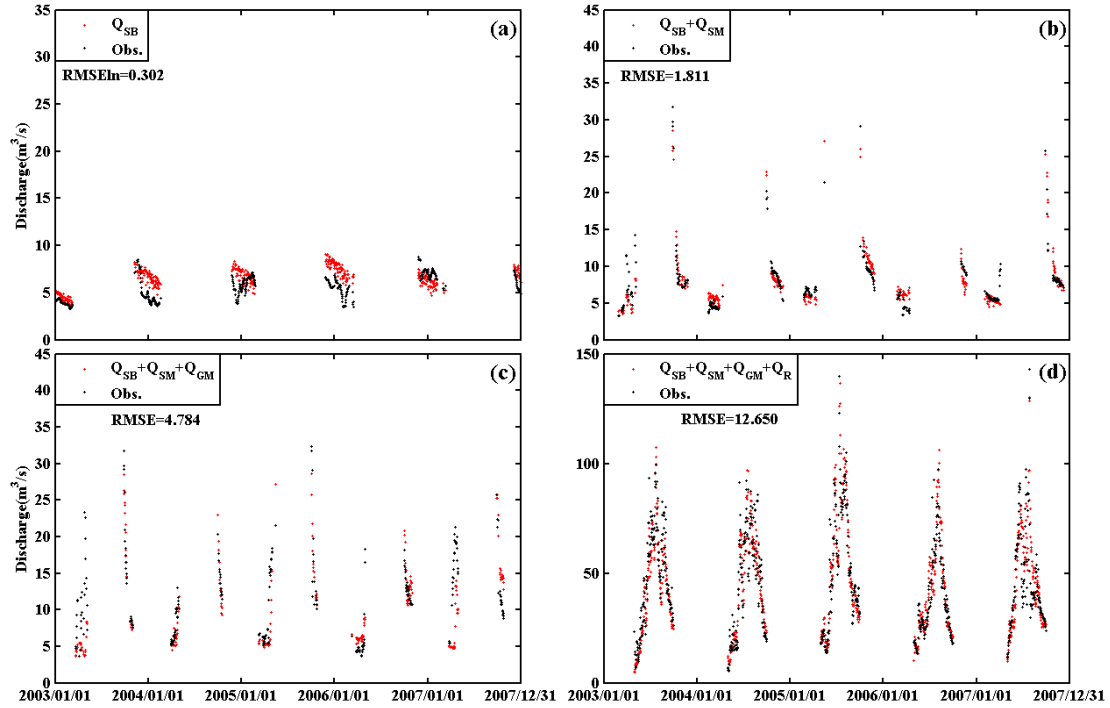
1075

1076

1077

1078

Figure 6. Hydrograph partition in 2003. Q_{SB} stands for subsurface baseflow generated by groundwater, Q_{SM} and Q_{GM} for snow meltwater and glacier meltwater respectively, and Q_R for rainwater directly runoff.



1079

1080

1081

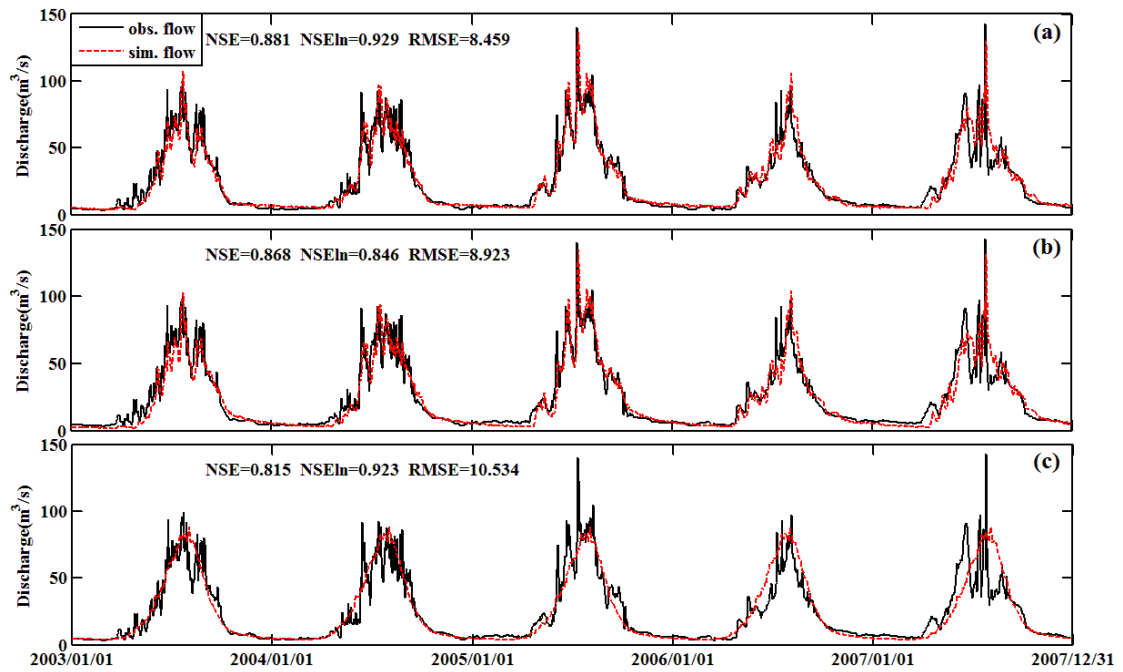
1082

1083

1084

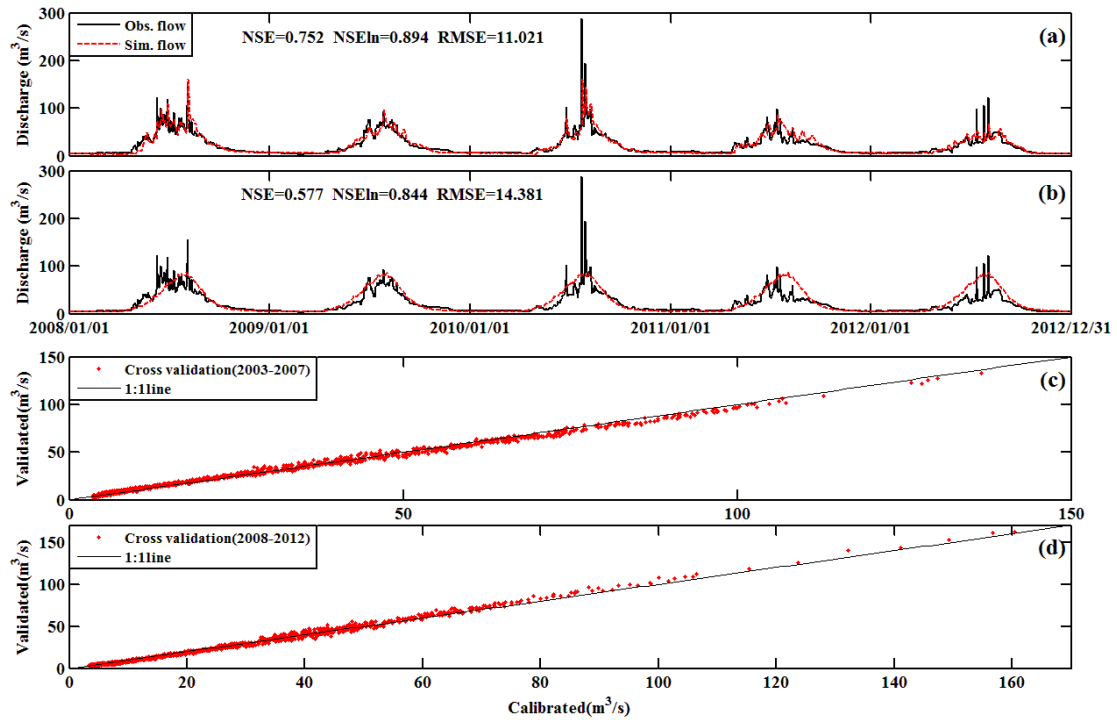
1085

Figure 7. Stepwise calibration of grouped parameters upon partitioning curves. (a) Partitioning curves after calibrating K_A and K_D upon Q_{SB} . (b) Partitioning curves after calibrating D_s upon $Q_{SB}+Q_{SM}$. (c) Partitioning curves after calibrating D_g upon $Q_{SB}+Q_{SM}+Q_{GM}$. (d) Partitioning curves after calibrating W_M and B upon $Q_{SB}+Q_{SM}+Q_{GM}+Q_R$. The goodness of fit between observed and simulated discharge is measured by $RMSEln$ (for Q_{SB} part) or $RMSE$ (for other parts).



1086
 1087
 1088
 1089

Figure 8. Simulation of daily streamflow by different methods from 2003 to 2007. (a) by the proposed stepwise method, (b) by the automatic calibration method, and (c) by the benchmark model. The performance of the simulations is measured in *NSE*, *NSEln* and *RMSE*.



1090

1091

1092

1093

1094

1095

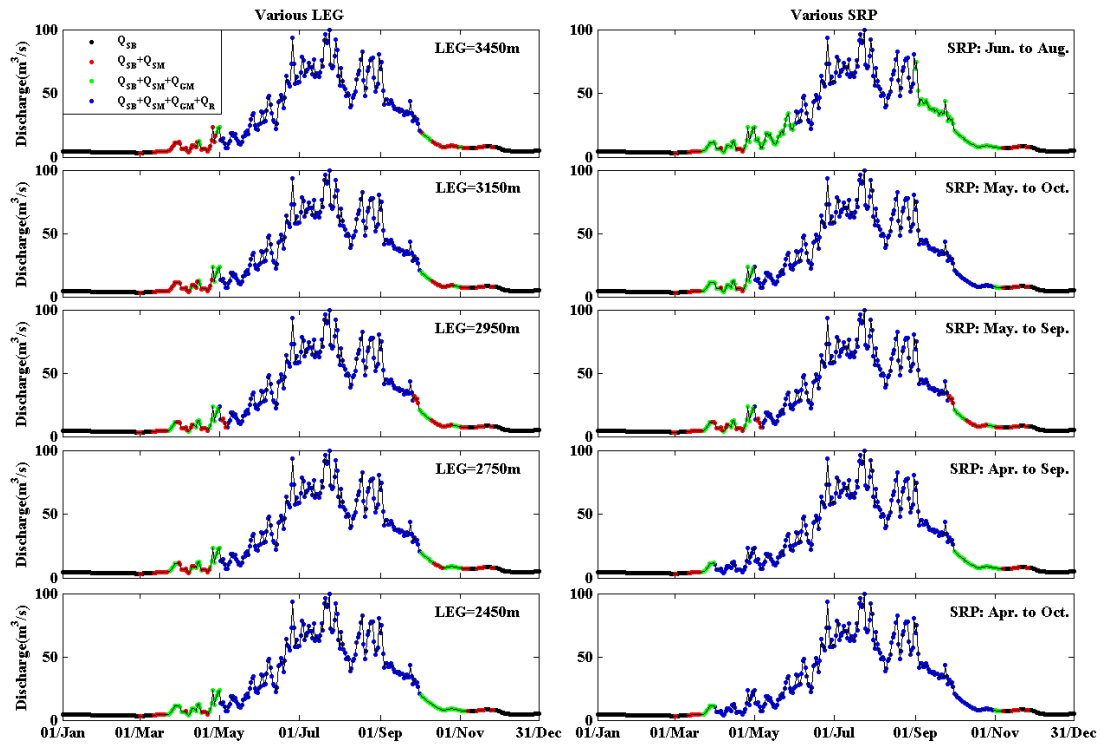
1096

1097

1098

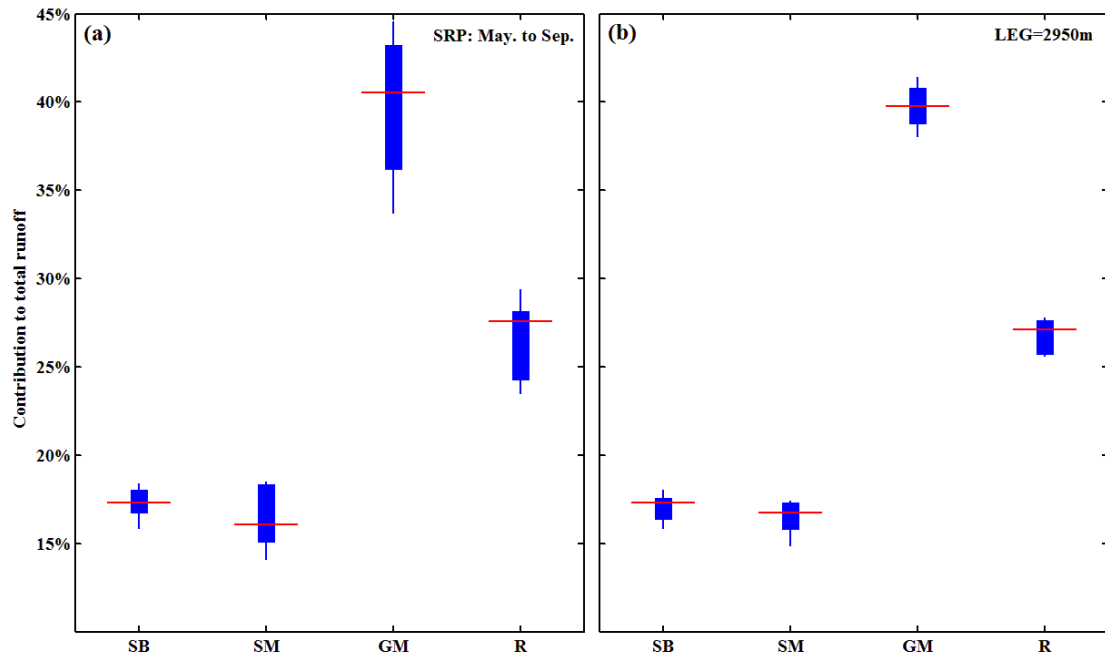
1099

Figure 9. Evaluation of the stepwise calibration method. (a) discharge simulation in evaluation period 2008 to 2012 using the stepwise calibrated parameters in calibration period 2003 to 2007. (b) discharge simulation in evaluation period 2008 to 2012 by the benchmark model. (c) Cross validation simulation of daily discharge in 2003-2007. x-coordinate presents the simulated daily discharges by parameters calibrated in period 2003-2007. y-coordinate presents the simulated daily discharges by parameters calibrated in period 2008-2012. (d) Cross validation simulation of daily discharge in 2008-2012. x-coordinate presents the simulated daily discharges by parameters calibrated in period 2008-2012. y-coordinate presents the simulated daily discharges by parameters calibrated in period 2003-2007.



1100
 1101
 1102
 1103
 1104

Figure 10. Sensitivity analysis for hydrograph partition. The first column is the hydrograph partition pattern using different lowest elevation band of the glacier area (LEG). The second column is the hydrograph partition pattern using different storm rain period (SRP).



1105
 1106
 1107
 1108
 1109
 1110
 1111
 1112

Figure 11. Sensitivity analysis on the contributions of different runoff sources to total runoff. (a) is the contribution pattern under different lowest elevation band of glacier area (LEG), where the storm rain period (SRP) is fixed as May to September. (b) is the contribution pattern under different SRPs, where the LEG is fixed as 2950m. The red line stands for the mean contribution for each runoff source, and the top/bottom end of each plot presents the highest/lowest contribution ratio. SB is groundwater baseflow, SM is snowmelt, GM is glacier melt and R is rainwater directly runoff.